THIN LINEAR-TO-CIRCULAR POLARIZERS WITH ENHANCED BANDWIDTH

by

Monique van den Berg

Submitted in partial fulfilment of the requirements for the degree
Master of Engineering (Electronic Engineering)

in the

Department of Electrical, Electronic and Computer Engineering
Faculty of Engineering, Built Environment and Information Technology

UNIVERSITY OF PRETORIA

January 2018

SUMMARY

THIN LINEAR-TO-CIRCULAR POLARIZERS WITH ENHANCED BANDWIDTH

by

Monique van den Berg

Supervisor: Prof J. Joubert

Co-supervisor: Prof. J.W. Odendaal

Department: Electrical, Electronic and Computer Engineering

University: University of Pretoria

Degree: Master of Engineering (Electronic Engineering)

Keywords: Enhanced bandwidth, frequency selective surface, linear-to-circular, metasurface, polarizer, polarization conversion, single-layer.

Circular polarization is valuable for many electromagnetic radiation applications such as wireless and satellite communication, radars, RFID, global positioning systems, etc. Many efforts have been made to manipulate and control polarization by using linear-to-linear or linear-to-circular transmission or reflection polarization converters. Most of the existing linear-to-circular single-layer polarizers have been found to be narrowband. Some attempts have been made to improve the bandwidth of these polarizers including using multiple layered structures at the expense of a bulkier device. There was, however, still a requirement for thin single-layer linear-to-circular polarizers with enhanced bandwidth. The purpose of this research was to design two thin single-layer linear-to-circular polarizers, one for transmission and the other for reflection, with enhanced bandwidth.

A thin single-layer linear-to-circular transmission polarizer with a 3 dB axial ratio bandwidth of 34% is presented. The bandwidth of this polarizer is significantly better than that of previously published polarizers of the same type. The unit cell of the polarizer consists of an

I-shaped strip and a perpendicular linear strip printed on the one side of a thin dielectric substrate and two additional capacitive coupling strips printed on the other side of the substrate. Experimental results were found to agree well with the simulated results.

A thin single-layer reflective linear-to-circular polarizer with a 3 dB axial ratio bandwidth of 57% is also presented. The unit cell of the polarizer consists of an I-shaped strip and a perpendicular linear strip printed on the one side of a substrate and a ground plane on the other side of the substrate. Experimental results for this polarizer were also found to agree well with the simulated results.

LIST OF ABBREVIATIONS

CST	Computer Simulation Technology
EM	Electromagnetic
EBG	Electromagnetic Band Gap
FSS	Frequency Selective Surface
MM	Metamaterial
MS	Metasurface
PCB	Printed circuit board
RCS	Radar Cross Section
VNA	Vector Network Analyser

TABLE OF CONTENTS

CHAPTER 1 INTRODUCTION

1.1 PROBLEM STATEMENT

1.1.1 Context of the problem and research gap

Circular polarization is valuable for many electromagnetic radiation applications such as wireless and satellite communication, radars, RFID, global positioning systems etc. [1]. Circular polarization in particular has been used to solve important challenges in wireless and satellite communication, such as vulnerability to multipath, atmospheric absorption, reflections and limiting interference from rain and fog [1], [2]. In satellite systems the effect of Faraday rotation can also be minimized by the use of a circularly polarized signal. In many antenna applications polarization diversity is desired and can be achieved by using circularly polarized signals [3].

Some effort has been made to manipulate and control polarization by using linear-to-linear or linear-to-circular transmission or reflection polarization converters. A few linear-to-linear transmission polarizers have been reported in the literature [4] - [6], and these polarizers all consist of multiple layers. These polarizers can be used to realize 90° polarization rotators [4]. In [4] a bi-layered transmission polarizer is proposed to convert incident linear polarization to its cross polarization. In [5] a three-layer polarizer is proposed where each layer consists of a complimentary split ring resonator rotated 45° in relation to the previous layer. The bandwidth of these polarizers can be increased by adding another layer but this is at the expense of a bulkier device.

Several single-layer linear-to-circular transmission polarizers have been reported in the literature [1], [2], [7] - [9]. These transmission linear-to-circular polarizers have been used to change the polarization of a source antenna from linear to circular, and also improve the performance of the source antenna, in terms of gain, return-loss bandwidth and radiation pattern [7]. In [8] the Radar Cross Section (RCS) of a slot antenna is reduced with such a polarizer. These single-layer linear-to-circular transmission polarization converters have been found to be relatively narrow band. A single-layer transmission polarizer with a unit cell consisting of two nested split ring slots was proposed in [8], with measured results showing a 3 dB axial ratio bandwidth of approximately 12%. Another polarizer with a metallic ring and a linear strip in the middle as unit cell was presented in [1], and a 3 dB axial ratio bandwidth of 17% was achieved. All these thin single-layer polarizers are only partially transmissive. In general, halve the incident power is transmitted and the other halve reflected. Polarizers like this can be used as superstrates for reflector backed linearly polarized antennas (e.g. patch antennas) with the aim of achieving circular polarization. The authors of [10], [11] improved the axial ratio bandwidth by using multiple layered structures, at the expense of a bulkier device.

Linear-to-linear reflective polarizers received significant attention in the literature [12] - [17]. These reflective linear-to-linear polarizers have been used as the ground plane of an antenna, to reflect the bottom lobe of the antenna and alter the reflected waves polarization to realize a circularly polarized radiator [14]. In [14] it was found that RCS reduction is also achieved as a result of using such a polarizer. Some effort, including using multiple plasmon resonances, have been made to provide linear-to-linear reflective polarizers with large 3 dB axial ratio bandwidths. A linear-to-linear polarizer with a double headed arrow on one side of a substrate and a ground plane on the other side was presented in [13], [14], and a 3 dB axial ratio bandwidth of 113.44% was achieved. Another linear-to-linear reflective polarizer with a unit cell consisting of an anchor shape was proposed in [15], with results showing a 3 dB axial ratio bandwidth of around 117%.

Only one single-layer linear-to-circular reflective polarizer could be found in the literature. This single-layer reflective linear-to-circular polarizer with a unit cell consisting of two

perpendicular I-shaped structures printed on top of a ground plane was presented in [18], with measured results showing a 3 dB axial ratio bandwidth of 25%.

When considering only results published for single-layer polarizers, it was observed that different unit cells produced polarizers with different axial ratio bandwidths. The bandwidth is thus dependent on the shape and characteristics of the unit cell. It might be possible to find a new unit cell or optimize an existing unit cell to achieve improved bandwidth, as there is still a requirement for single-layer linear-to-circular polarizers with improved bandwidth.

1.2 RESEARCH OBJECTIVE AND QUESTIONS

The objective of this research was to design **two** thin single-layer linear-to-circular polarizers with enhanced bandwidth. The aim was to design one transmission type polarizer, and one reflection type polarizer. The two polarizers should perform better than existing single-layer linear-to-circular polarizers, in terms of axial ratio bandwidth.

Questions that arose when considering the problem statement and the research objectives included:

- What axial ratio bandwidth is achieved in the literature by single-layer linear-to-circular polarizers?
- How large can the bandwidth of a thin linear-to-circular polarizer be made?

1.3 APPROACH

A systematic approach was followed to design the transmission polarizer. A literature study on transmission polarizers was completed. A few single-layer linear-to-circular transmission polarizers mentioned in the literature [1], [2], [7] - [9] were simulated with the aid of the commercial simulation software CST (Computer Simulation Technology) Microwave Studio^{TM}. These polarizers were simulated to determine their functionality and what kind of bandwidth single-layer transmission polarizers available achieve. The Jerusalem-cross

polarizer presented in [2] was chosen as the basis of this research. A parametric study was performed on the Jerusalem-cross polarizer to determine whether an improvement in axial ratio bandwidth could be achieved. An equivalent circuit was used to model the transmission of a vertically or horizontally polarized plane wave (normally incident) through a planar Jerusalem-cross array. Using the knowledge gained from studying the equivalent circuit model and performing a parametric study, a new unit element was derived. The new unit element was designed based on the hypothesis that altering the geometry of the unit cell to increase the bandwidth of the unit cell, will also increase the bandwidth of the linear-to-circular polarizer. The transmission polarizer unit element was then simulated and optimized in CST. A numerical experiment was performed to determine whether a finite sized polarizer could be physically tested. The transmission polarizer was manufactured and then tested in a compact antenna range. The measured results were compared to the simulated results. The simulated axial ratio bandwidth was also compared to the simulated axial ratio bandwidth of the transmission polarizers mentioned in [1], [2], [7] - [9].

A similar approach was followed to design the reflective polarizer. A literature study on reflective polarizers was conducted. A single-layer linear-to-circular reflective polarizer mentioned in the literature [18] was simulated with the aid of the commercial simulation software CST. The polarizer was simulated to determine its functionality and what kind of bandwidth single-layer reflective polarizers available achieve. The polarizer presented in [18], which consists of two orthogonal I-shaped structures, was chosen as the basis of the polarizer design. A parametric study was performed on this polarizer to determine whether an improvement in axial ratio bandwidth could be achieved. An equivalent circuit was used to model the reflection of a vertically or horizontally polarized plane wave (normally incident) by a planar ground backed Jerusalem-cross array. A new unit element was designed based on the hypothesis that altering the geometry of the unit cell to increase the bandwidth of the unit cell, will also increase the bandwidth of the linear-to-circular polarizer. The reflective polarizer unit element was then simulated and optimized in CST. The reflective polarizer was manufactured and then tested in a compact antenna range. The measured results were compared with the simulated results. The simulated axial ratio bandwidth was

also compared with the simulated axial ratio bandwidth of the reflective linear-to-circular polarizer presented in [18].

1.4 RESEARCH GOALS

The following goals were set in the designing and testing of the two polarizers with enhanced axial ratio bandwidth; (i) the polarizers had to perform better in terms of axial ratio bandwidth than other single-layer polarizers found in the literature, (ii) the polarizers had to be easy to manufacture , it must be etched with a normal Printed circuit board (PCB) etching process and have realizable dimensions, (iii) each polarizer's performance had to be tested by measuring the manufactured polarizer data and comparing it to the simulated results.

1.5 RESEARCH CONTRIBUTION

The contributions made through the work presented in this dissertation are listed below.

A thin single-layer linear-to-circular transmission polarizer with enhanced bandwidth: The proposed polarizer's unit cell was derived from a conventional Jerusalem-cross geometry [2]. By altering the dimensions of the two I-shaped structures which form the Jerusalem-cross, the two pairs of resonances due to orthogonal linear plane wave excitation of the polarizer can be controlled almost independently. By adjusting the locations of the resonances, the frequency range across which the magnitudes of the components of the linear plane wave are equal and the phase difference between the components is 90° can be increased, and as such the circular polarization axial ratio bandwidth can also be increased.

A thin single-layer reflective linear-to-circular polarizer with enhanced bandwidth: The proposed polarizer's unit cell was derived from a conventional ground backed Jerusalem-cross geometry [18]. By altering the dimensions of the two I-shaped structures which form the Jerusalem-cross, the frequency range across which the magnitudes of the components of a linear plane wave excitation are equal and the phase difference between the

components is 90° can be increased, and as such the circular polarization axial ratio bandwidth can also be increased.

1.6 OVERVIEW OF STUDY

The organisation of the dissertation is as follows:

Chapter 2 provides some background information on polarizers. The question of how to classify periodic composite materials is also discussed. The different transmission and reflection polarizers found in the literature are presented. Methods used to increase the bandwidth of these polarizers are discussed.

In Chapter 3 the performance of five linear-to-circular transmission polarizers and one reflective linear-to-circular polarizer, mentioned in the literature, is studied.

In Chapter 4 the design of the single-layer linear-to-circular transmission polarizer is presented. The polarizer's simulation results are also shown in this chapter.

Chapter 5 presents the measured results of the proposed linear-to-circular transmission polarizer. This chapter also contains a comparison of the simulated results with the simulated results of five-scaled linear-to-circular transmission polarizers found in the literature. A discussion of the measured results is also included in this chapter.

In Chapter 6 the design of the single-layer linear-to-circular reflective polarizer is presented. The polarizer's simulation results are also shown in this chapter.

Chapter 7 presents the measured results of the proposed linear-to-circular reflective polarizer. This chapter also contains a comparison of the simulated results with the simulated results of a single linear-to-circular reflective polarizer found in the literature. A discussion of the measured results is also included in this chapter.

The last chapter, Chapter 8, provides an overview of the work performed. Possible future work is also mentioned.

CHAPTER 2 LITERATURE STUDY

2.1 CHAPTER OBJECTIVES

This chapter provides background information on polarizers and studies the different transmission and reflection polarizers found in the literature. In Section 2.2 background information on polarizers are provided. In Section 2.3, the classification of periodic composite materials is discussed. In Section 2.4 the different transmission polarizers found in the literature are investigated. In this section the methods used to increase the bandwidth of these polarizers are also discussed. In Section 2.5 different reflection polarizers are investigated, and methods used to increase the bandwidth of these polarizers are also discussed. In Section 2.6 the chapter is concluded.

2.2 POLARIZERS

Transmission or reflection polarization converters can be used to manipulate and control polarization. As a linearly polarized incident wave travels through, or is reflected by a polarizer, a cross- or circularly polarized output wave can be obtained. To achieve a linear-to-circular polarization change the aim is to achieve equal magnitude transmission or reflection for two incident orthogonal linear components (of a linearly polarized incident wave), but with a 90° phase difference between the components.

These polarizers are constructed as periodic composite materials - low loss dielectric sheets with a rectangular array of printed metallic structures on one side of the dielectric sheet and or a ground plane on the other side. Incident energy is redirected because of interference and diffraction, and because of the asymmetry of the unit elements the transmission or reflection

characteristics are also dependent on the polarization of the incident wave. Polarizers are not polarization independent. For polarization conversion the incident fields' polarization must be very specifically aligned with the unit elements' orientation.

These polarizers can be regarded as a Frequency Selective Surface (FSS), but are also sometimes referred to as a Metasurface (MS). A perspective on the difference between an MS and an FSS is described in some detail in [3] and will be discussed in the next section.

2.3 CLASSIFICATION

Periodic composite materials can be categorized based on the periodicity of the structure in relation to the wavelength, and the nature of the resonances associated with the individual scatterers or the lattice periodicity [3]. Composite materials can be separated into three regions, as summarized in Table 2.1.

Consider three dimensional composite materials. At low frequencies, where the period of the structure (periodicity of the scatterers) is much smaller than the wavelength of operation, the composite material falls in Region 1, which is known as the Quasi-static region. In this region the effective material properties can be obtained using classical mixing formulas [3].

Region 2 corresponds to the region where the scatterers themselves resonate (but not the lattice) and the period of the structure is still small compared to the wavelength. A composite material which falls in this region is defined as a Metamaterial (MM).

In Region 3, the composite material is no longer seen as an effective medium, and the period of the structure is now comparable to or larger than the wavelength of operation. At these frequencies a full wave approach must be used to determine the interaction of the Electromagnetic (EM) field with the composite material. The Floquet-Bloch mode expansion can be used for this purpose [3].

Higher order Floquet-Bloch modes must be considered as the period of the structure approaches the wavelength of operation. The fundamental wave propagating through the composite material is affected by these higher order modes, and at these frequencies the composite material is defined as an Electromagnetic Band Gap (EBG) material.

For a two-dimensional composite material which consists of a lattice of scatterers, Region 1 corresponds to classical thin film materials. A composite material which falls in Region 2 is defined as an MS. In this region the scatterers themselves resonate (but not the lattice). Region 3 corresponds to the region where the resonances are associated with the periodicity of the scatterers. Conventional FSSs form part of this region.

In summary in Region 1 and Region 2 the composite material is treated as an effective medium. The effective material properties of the composite material are not frequency dependent in Region 1. In Region 2 the effective material properties are frequency dependent. In Region 3 the periodicity of the lattice influences the EM response of the composite material. The same composite material can be treated as three different media operating in three different frequency regions [3].

Table 2.1 Three operating regions of composite materials [3].

Region 1	**Region 2**	**Region 3**
Effective media	Dispersive effective media	Not seen as an effective medium
Classical mixing theory		Floquet-Bloch mode analysis
	Scatterers themselves resonate (but not the lattice)	Resonances associated with the periodicity of the scatterers
	MM/MS	FSS

It is not always easy to make a definitive decision if a particular polarizer surface should be classified as an MS (region 2) or an FSS (region 3). There will also be a gradual transition in the properties as the frequency increases, and therefore all polarizers in this dissertation will be regarded as surfaces that may have properties of region 2 and or region 3. For this reason, all the analysis results in this dissertation were generated with CST Microwave Studio using the "unit cell" boundary condition and Floquet ports, which is capable of accurately analyzing region 3 surfaces.

2.4 TRANSMISSION POLARIZERS

In this section different transmission polarizers found in the literature are investigated. Only polarizers which consist of a repeating pattern etched on top of a substrate are considered. In this section the methods used in the literature to improve the bandwidth of these polarizers are also mentioned.

2.4.1 Linear-to-linear

A bi-layered transmission polarizer was proposed in [4], to convert incident linear polarization to cross polarization. The top layer consists of four identical cut-wires which form a square. The bottom layer is a horizontally flipped mirror image of the top layer. The unit cell is shown in Fig. 2.1**.** .

The polarizer, when excited with a horizontally directed linearly polarized wave, generates a vertically directed wave after transmission. The proposed structure can be viewed as the combination of four cut-wire pairs. A magnetic dipole is excited by the magnetic field of a cut-wire pair. The magnetic dipoles in the four cut-wire pairs are strongly coupled to each other. Due to this coupling, cross-polarization transmission is obtained. The polarizer achieves a polarization conversion efficiency of 90%.

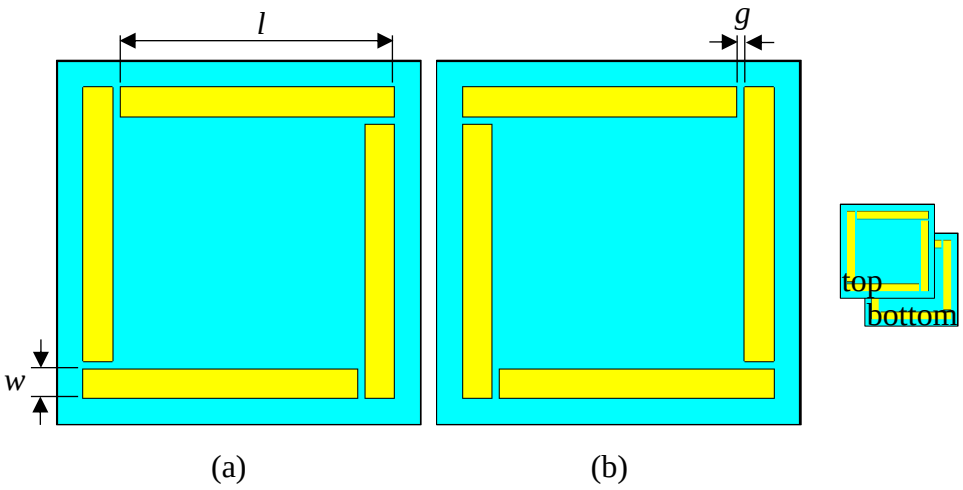

Fig. 2.1. Square cut wire unit cell [4].

(a) Front view of top layer. (b) Front view of bottom layer.

In [5] a three-layer polarizer was proposed to convert incident linear polarization to cross polarization. Each layer consists of a complimentary split ring resonator, rotated 45° in relation to the previous layer. The unit cell is shown in Fig. 2.1.

The polarizer was excited with a horizontally polarized linear wave, and after transmission a vertically polarized wave was achieved. The polarizer achieves a bandwidth of 24% and a polarization conversion efficiency of 96%.

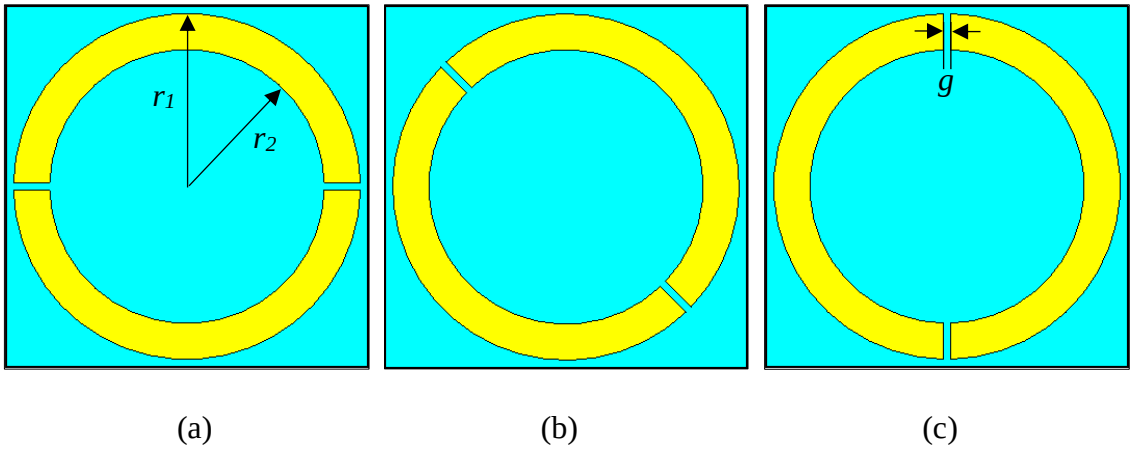

Fig. 2.1. Complimentary split ring resonator unit cell [5].

(a) Front view of top layer. (b) Front view of middle layer. (c) Front view of bottom layer.

A bi-layered transmission polarizer was proposed in [6] to convert incident linear polarization to cross polarization. The top layer consists of an asymmetrically split ring aperture. The bottom layer is a 90° rotated version of the top layer. The unit cell is shown in Fig. 2.2.

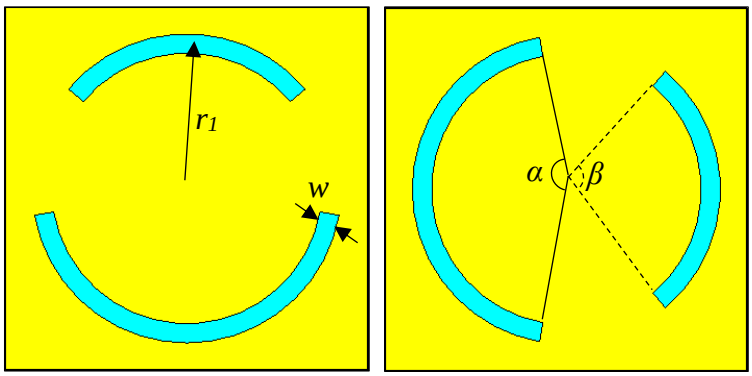

(a) (b)

Fig. 2.2. Asymmetric split ring aperture unit cell [6].

(a) Front view of top layer. (b) Front view of bottom layer**.**

The polarizer, if excited with a vertically polarized linear wave, yields a horizontally polarized wave after transmission. The polarizer achieves a bandwidth of 58% with almost zero copolarization transmission.

2.4.2 Linear-to-circular

A single-layer linear-to-circular transmission polarizer with a unit cell consisting of two nested split ring slots (shown in Fig. 2.3) was proposed in [8]. The measured 3 dB axial ratio bandwidth obtained with this design was 11.75%.

The polarizer was excited with a 45° linearly polarized wave, which is the superposition of a vertical and horizontal polarized wave (E_1 and E_2) of equal magnitude and phase. A circularly polarized output signal could be obtained because the polarizer advances the phase of one component of the incident wave by plus 45° and retards the phase of the other

component by minus 45° (phase difference of 90° between the components) while at the same time producing components of equal magnitude.

The amplitude and phase of the transmitted signals could be controlled by the length, width and spacing of the inner and outer slots. The dimensions of the two nested split rings slots were selected in such a manner that the vertically polarized incident wave would cause the longer outer slot to resonate slightly below the centre frequency, while the horizontally polarized incident wave would cause the shorter inner slot to resonate at a frequency slightly above the centre frequency. At the centre frequency of 325 GHz the length of both slots was close to one wavelength. The unit cell size is 0.515 by $0.585\lambda^2$ [8].

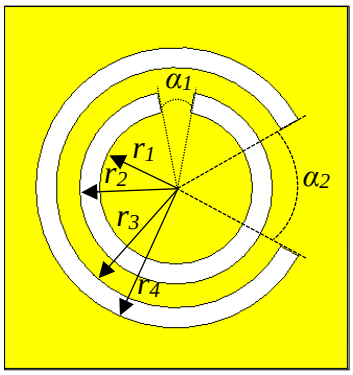

Fig. 2.3. Two nested split ring slots unit cell [8].

Fig. 2.4 shows a single-layer transmission linear-to-circular polarizer with a Jerusalem-cross based unit cell [2]. A 3 dB axial ratio bandwidth of 4.3%, around the centre frequency of 17.8 GHz, was demonstrated by this design.

A 45° linearly polarized wave, which is the superposition of a vertical and horizontal polarized wave (E_1 and E_2) of equal magnitude and phase, was chosen as the excitation. Circular polarization could be achieved by adjusting the lengths L_1, L_2, L_3 and L_4 to provide inductive and capacitive coupling between unit cells which facilitated a 90° phase difference between the vertical and horizontal components. The unit cell size is 0.33 by $0.33\lambda^2$ [2].

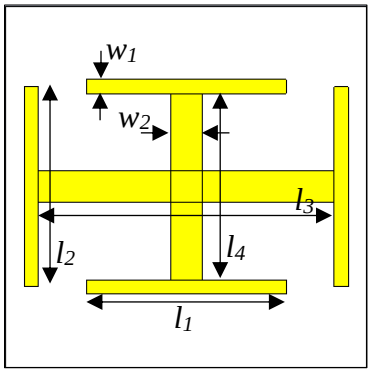

Fig. 2.4. Jerusalem-cross unit cell [2].

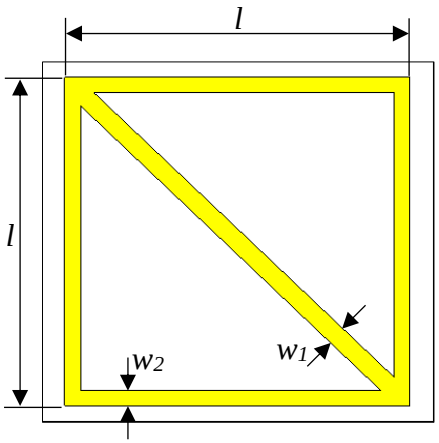

Fig. 2.5. Rectangular loop and diagonal strip unit cell [7].

Fig. 2.5 shows a single-layer metasurface transmission polarizer with a unit cell consisting of a rectangular loop and a diagonal strip [7]. The polarizer was used to alter the polarization and improve the return loss bandwidth and gain of a patch and slot antenna. The measured 3 dB axial ratio bandwidth obtained with this polarizer design was 12% around the centre frequency of 2.45 GHz

The polarizer was excited with a vertical linearly polarized wave, which is the superposition of a plus 45° wave and a minus 45° wave (E_1 and E_2) of equal magnitude and phase. The two components could be phase advanced and delayed by the inductive and capacitive effects of the diagonal strip and rectangular loop, due to the fact that the one component was parallel to the diagonal strip and the other component was perpendicular to the diagonal strip.

If the phase difference between the components is 90°, a circular polarized signal can be obtained. The unit cell size is 0.38 by $0.38\lambda^2$ [7].

In [8] a single-layer metasurface transmission polarizer with a unit cell consisting of an asymmetric cross slot was presented. The unit cell is shown in Fig. 2.6. The polarizer was used to reconfigured the polarization of a slot antenna and simultaneously reduce the RCS of the antenna. A 3 dB axial ratio bandwidth of 10% was demonstrated by this polarizer design around a centre frequency of 4.4 GHz.

A vertical linearly polarized wave was used to excite the polarizer. This wave is the superposition of a plus 45° wave and a minus 45° wave (E_1 and E_2) of equal magnitude and phase. This wave causes both arms of the cross slot to resonate simultaneously. By adjusting the lengths of the two slots, the reactance of the polarizer can be controlled to produce signals of equal magnitude with a phase difference of 90°, circularly polarized signals could be obtained. The unit cell size is 0.137 by $0.137\lambda^2$ [8].

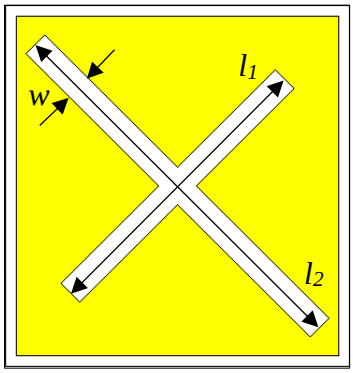

Fig. 2.6. Cross slot unit cell [8]**.**

Fig. 2.7 shows a polarizer with a metallic ring and a linear strip in the middle as unit cell [1]. A 3 dB axial ratio bandwidth of about 17% was achieved with this design. This polarizer was used as the superstrate of a linearly polarized microstrip patch antenna.

The polarizer was excited with a vertically orientated linearly polarized wave, and after transmission a circularly polarized output wave was obtained. The unit cell size is 0.462λ by 0.462λ at a centre frequency of 14.45 GHz [1].

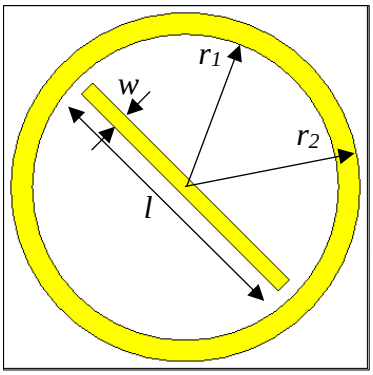

Fig. 2.7. Unit cell consisting of a metallic ring with linear strip in the middle [1].

2.4.2.1 Improved bandwidth

In [10] a bi-layered MS polarizer was used to achieve an axial ratio bandwidth of 60% around a centre frequency of 14.65 GHz. The MS is composed of two layers of metallic pattern arrays etched on opposite sides of a substrate, shown in Fig. 2.8. The polarizer achieves polarization conversion transmission of 90% across the 11 GHz to 18.3 GHz frequency range.

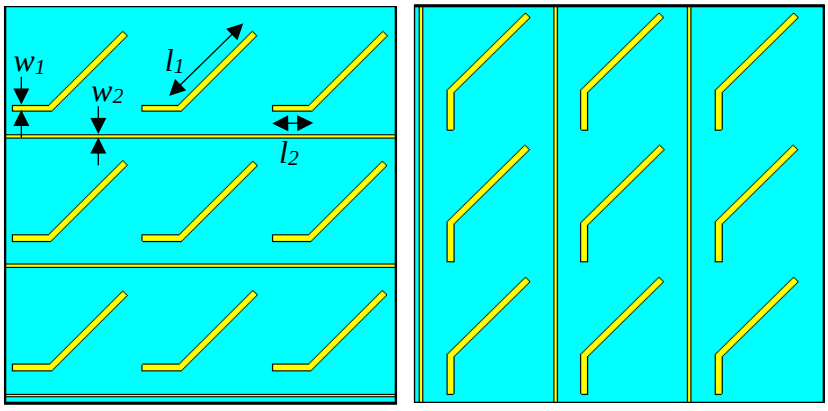

(a) (b)

Fig. 2.8. Metallic pattern array unit cell [10].

(a) Front view of top layer. (b) Front view of lower layer.

A four-layer FSS air spaced transmission linear-to-circular polarizer was proposed in [11]. A 3 dB axial ratio bandwidth of 57.55% was achieved with this design. The unit cell is a split ring resonator bisected by a metal strip, shown in Fig. 2.9. The bandwidth of the polarizer was increased by cascading the FSSs.

The polarizer was excited with a 45° linearly polarized wave. The horizontal component was mainly affected by the capacitive effect of the horizontal gaps. The vertical component was mainly affected by the inductive effect of the metallic strip. As a result, there was a phase difference between the vertical and horizontal components. A circularly polarized transmitted wave could be obtained if both the spacing between the layers and the dimensions were adjusted to obtain a 90° phase difference between the vertical and horizontal components.

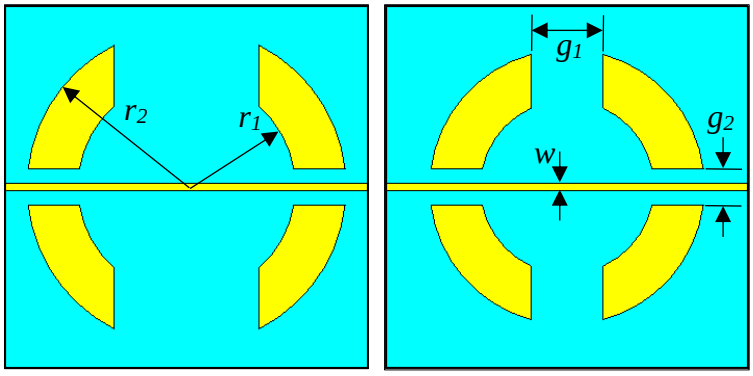

(a) (b)

Fig. 2.9. Split ring resonator bisected by a metal strip unit cell [11].

(a) Front view of inner layers. (b) Front view of outer layers.

In [19] a three-layer polarizer, which is based on a second order bandpass FSS, was proposed and used to achieve an axial ratio bandwidth of 30%. The unit cell consists of two aperture coupled patches, shown in Fig. 2.10. A circularly polarized wave was obtained after transmission from a vertically or horizontally polarized incident wave.

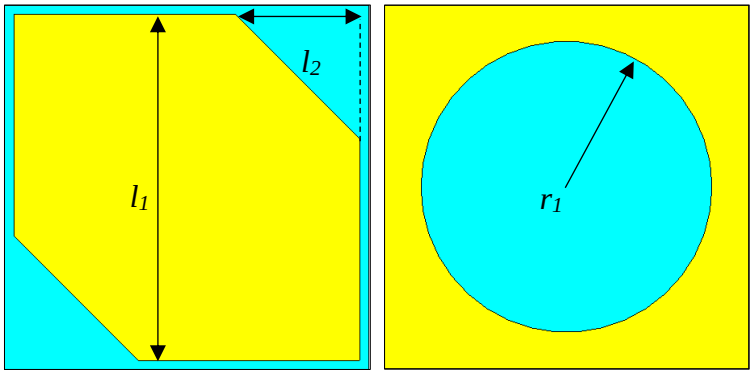

(a) (b)

Fig. 2.10. Two aperture coupled patches unit cell [19].

(a) Front view of top and bottom layer. (b) Front view of middle layer.

2.5 REFLECTIVE POLARIZERS

In this section different reflective polarizers found in the literature are investigated. Only polarizers which consist of a repeating pattern etched on top of a substrate and a ground plane on the other side of the substrate are considered. In this section the methods used in the literature to improve the bandwidth of these polarizers are also mentioned.

2.5.1 Linear-to-linear

A reflective polarizer with a wide operating band is proposed in [12]. Multiple plasmon resonances are used to achieve a high conversion efficiency and a wide operating band. The unit cell is composed of two concentric asymmetric split ring resonators on one side of a substrate and a ground plane on the other side, as shown in Fig. 2.11.

The polarizer was excited with a vertical linearly polarized wave, which is the superposition of two orthogonal components (E_1 and E_2) of equal magnitude and phase. Three plasmon resonance eigen-modes are excited by a vertical linearly polarized incident wave, two eigen-modes are excited by E_1 which is perpendicular to the split gap and one eigen-mode is excited by E_2 which is parallel to the split gap. The cross-polarization reflection bandwidth can be

extended by shifting the three plasmon resonances. The location of the resonances can be tailored by altering the dimensions of the unit cell.

The resonant frequencies are located at 9.57 GHz, 10.6 GHz and 12.02 GHz. A polarization conversion efficiency of 99% is achieved across the 9.1 GHz to 12.9 GHz frequency range. A 3 dB bandwidth of 66.7% is achieved with this reflective linear-to-linear polarizer [12].

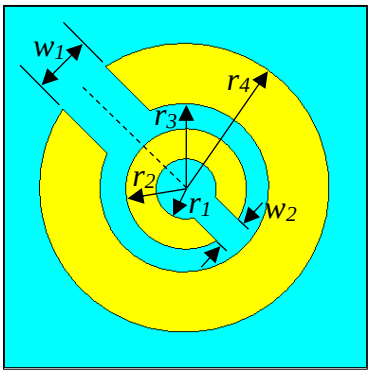

Fig. 2.11. Two concentric asymmetric split ring resonators unit cell [12].

A reflective linear-to-linear MS polarizer with a broad operating band, achieved with multiple plasmon resonances, was proposed in [13, 14]. The unit cell consists of a double headed arrow on one side of a substrate and a ground plane on the other side, shown in Fig. 2.12.

The polarizer was excited with a vertical linearly polarized wave, which is the superposition of two orthogonal components (E_1 and E_2) of equal magnitude and phase. Four plasmon resonance eigen-modes are excited by the vertically orientated linearly polarized incident wave, two eigen-modes are excited by E_1 which is parallel to the arrow and two eigen-mode are excited by E_2 which is perpendicular to the arrow. A wide operating band can be obtained by adjusting the locations of the four plasmon resonances. After reflection a horizontally orientated linearly polarized wave is obtained.

The 3 dB bandwidth achieved with this design is from 6.6 GHz to 23.9 GHz (113.44%) for both vertical and horizontal linearly polarized incident waves. The four resonances are

located at 6.8 GHz, 12.17 GHz, 15.45 GHz and 23.13 GHz. A polarization conversion ratio of 50% is achieved across the 3 dB band.

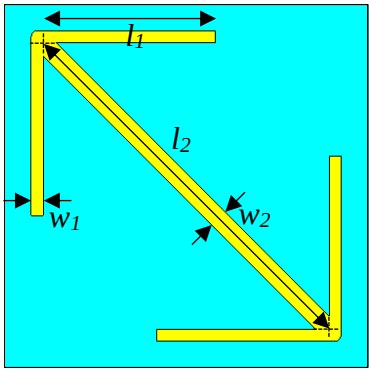

Fig. 2.12. Double headed arrow unit cell [13, 14].

A linear-to-linear reflective MS polarizer with a wide operating band was proposed in [15]. In this case five plasmon resonances are used to achieve polarization selectivity, incident angle insensitivity and a wide operating band. The unit cell is composed of an anchor shape on one side of a substrate and a ground plane on the other side, as shown in Fig. 2.13.

This design's 3 dB bandwidth is from 6 GHz to 23 GHz (117.24%) for both vertical and horizontal linearly polarized incident waves. Only vertical and horizontal linearly polarized incident waves can be converted to its orthogonal direction. The five plasmon resonances are located at 6.6 GHz, 9 GHz, 16 GHz, 19.6 GHz and 22.3 GHz. The polarization conversion ratio is 80% within the 3 dB bandwidth. The polarizer still performs well when the incident angle increases.

A reflective linear-to-linear MS polarizer with a broad operating band, achieved with four plasmon resonances, is proposed in [16]. The unit cell consists of four v-shaped resonators on one side of a substrate and a ground plane on the other side, as shown in Fig. 2.14.

A 3 dB bandwidth of 102.19% from 6.7 GHz to 20.7 GHz is achieved with this design. The four plasmon resonances are located at 7.5 GHz, 12.22 GHz, 16.64 GHz and 20.3 GHz. A polarization conversion ratio of 50% is achieved across the 3 dB band.

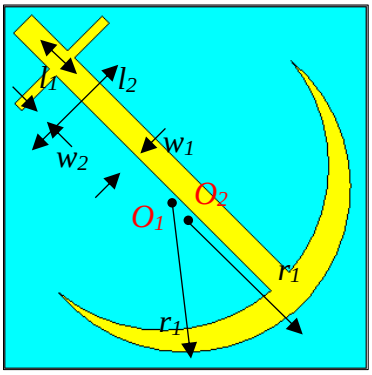

Fig. 2.13. Anchor shaped unit cell [15].

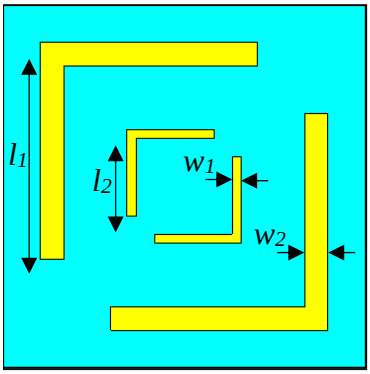

Fig. 2.14. V-shaped resonator unit cell [16].

In [17] a polarization control MS is proposed to reduce the RCS of a slot array antenna. The unit cell of the polarization control MS consists of a fishbone pattern on one side of a substrate and a ground plane on the other side, shown in Fig. 2.15.

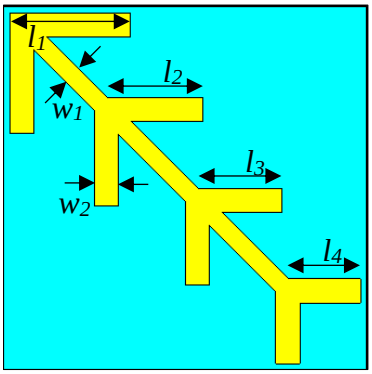

Fig. 2.15. Fishbone pattern unit cell [17].

Three plasmon resonances can be excited by a horizontal linearly polarized incident wave. The three resonances are located at 6 GHz, 11.5 GHz and 16 GHz. This design's 3 dB bandwidth is from 5.5 GHz to 17.5 GHz (104.35%), across which a horizontal linearly polarized incident wave will be converted to a vertical linearly polarized wave.

2.5.2 Linear-to-circular

A single-layer reflective linear-to-circular polarizer with a unit cell consisting of two perpendicular I-shaped structures printed on top of a ground plane (shown in Fig. 2.16) was presented in [18], with measured results showing a 3 dB axial ratio bandwidth of 25% was achieved.

The polarizer was excited with a 45° orientated linearly polarized wave, which is the superposition of two orthogonal components (E_{s1} and E_{s2}) of equal magnitude and phase. The two orthogonal components are parallel to the two I-shaped structures. By altering the dimensions of l_3 and l_4 the phases of E_{s1} and E_{s2} can be controlled independently. By varying the phase difference between E_{s1} and E_{s2}, the polarization state of the reflected wave can be manipulated. A circularly polarized reflected wave can be obtained when the phase difference is 90° (with equal magnitude) and a cross-polarized reflected wave can be obtained when the phase difference is 180°.

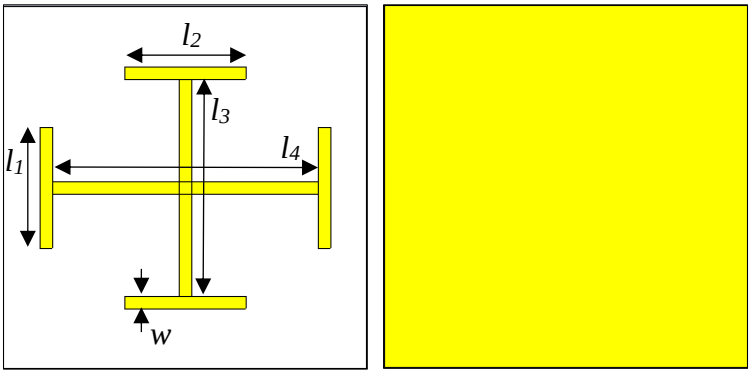

(a) (b)

Fig. 2.16. Two perpendicular I-shaped structures on top of a ground plane unit cell. (a) Front view. (b) Back view. [18]

2.6 CHAPTER SUMMARY

A perspective on the difference between an MS and an FSS has been presented. The difference has to do with the nature of the resonances in this case [3]. In MSs the scatterers themselves resonate (but not the lattice). In conventional FSSs the resonances are associated with the periodicity of the scatterers.

The single-layer polarizers mentioned were all excited by a 45° orientated, with reference to the symmetry plane of the unit elements, linearly polarized incident wave. This angled incident wave is required to facilitate the transformation from linear to circular. This is a limitation of all single-layer linear-to-circular polarizers.

When considering the single-layer polarizers presented in this section, it can be seen that different unit cells produce polarizers with different axial ratio bandwidths. The axial ratio bandwidth is dependent on the shape of the unit cell. It might be possible to find a new unit cell or optimize an existing unit cell for even better axial ratio bandwidth.

Due to the fact that all these polarizers operate at different frequencies and are implemented on different substrates, a direct comparison cannot be made. It is required that all the single-layer linear-to-circular polarizers are designed to operate at the same frequency, and implemented on the same substrate, to facilitate direct comparison. This was done in the next section, Chapter 3.

CHAPTER 3 SIMULATION STUDY

3.1 CHAPTER OVERVIEW

In this chapter the performance of the linear-to-circular polarizers described in Section 2.4 and Section 2.5 is studied and compared. To study the performance of these different polarizers on an equal and comparable basis, the unit cell used in each polarizer was modelled and simulated in CST.

3.2 LINEAR-TO-CIRCULAR TRANSMISSION POLARIZERS

A unit cell can be analysed by using the unit cell boundary condition and Floquet ports. The unit cell is duplicated an infinite number of times in the *X*-*Y* plane of the global coordinate system when the unit cell boundary condition is used. An array can be simulated using only a single unit cell and the unit cell boundary condition. Floquet ports are used to excite the unit cell on a specific side and determine the resulting S-parameters. The performance of the array can be determined from the S-parameters [20].

The polarizers were all designed to operate at the same frequency, 2.45 GHz, and implemented on the same substrate, to facilitate direct comparison.

Each polarizer was excited by a 45° linearly polarized wave, which consists of the superposition of a horizontally and vertically polarized wave with equal magnitudes and phase. In order to achieve circular polarization, the polarizer must produce a 90° phase difference between the horizontal and vertical components, while the magnitudes of these components remain equal.

Five linear-to-circular transmission polarizers are studied, namely: the nested split ring slot polarizer, the Jerusalem-cross polarizer, the rectangular loop with a diagonal microstrip polarizer, the cross-slot polarizer and the metallic ring with embedded rectangular strip polarizer. The dimensions and simulated results of the five polarizers are presented below.

3.2.1 Nested split ring slot polarizer

In [8] dimensions were provided for a nested split ring slot unit cell which operates at 325 GHz. CST was used to optimize these dimensions, to create a nested split ring slot unit cell which operates at 2.45 GHz. The dimensions were optimized for a phase difference of 90° between the horizontal and vertical components and -3 dB (equal) magnitude at 2.45 GHz. The thickness of the substrate and the substrate material were also varied.

The nested split ring slot unit cell is shown in Fig. 2.3. The substrate material is Rogers 4003C with ε_r = 3.38, tan δ = 0.0027 and thickness h = 0.813 mm. The determined dimensions for a centre frequency of 2.45 GHz are r_1 = 14.93, r_2 = 18.93 mm, r_3 = 23.46 mm, r_4 = 27.46 mm, α_1 = 22.11 degrees and, α_2 = 58.23 degrees. The period of the unit cell is 67.10 mm and 70.64 mm in the horizontal and vertical directions respectively.

Fig. 3.1 shows the transmission amplitude of the vertical and horizontal components across the 2 GHz to 3 GHz frequency range. It can be seen from Fig. 3.1 that the point of equal magnitude and equal power transmission is at 2.45 GHz.

Fig. 3.2 shows the phase difference between the horizontal and vertical components of the nesled split ring slot polarizer, across the 2 GHz to 3 GHz frequency range. It can be seen from Fig. 3.2 that the phase difference is 90° at 2.45 GHz, which is exactly at the frequency where equal magnitude and equal power transmission is achieved.

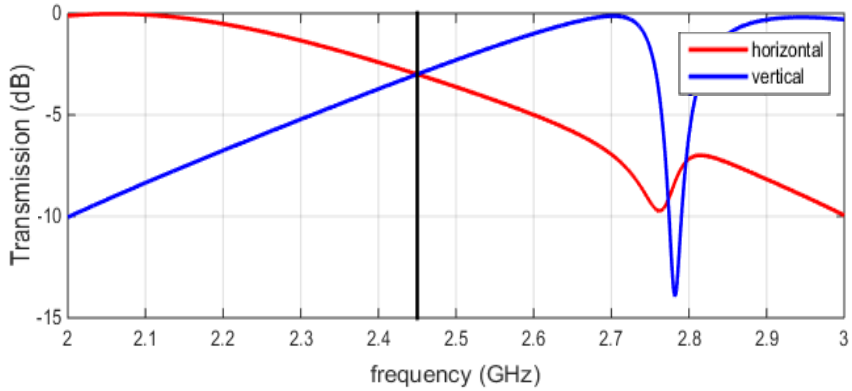

Fig. 3.1. Transmission amplitude as a function of frequency for the nested split ring slot polarizer. The vertical black line indicates the 2.45 GHz point where equal magnitude is required (- 3 dB).

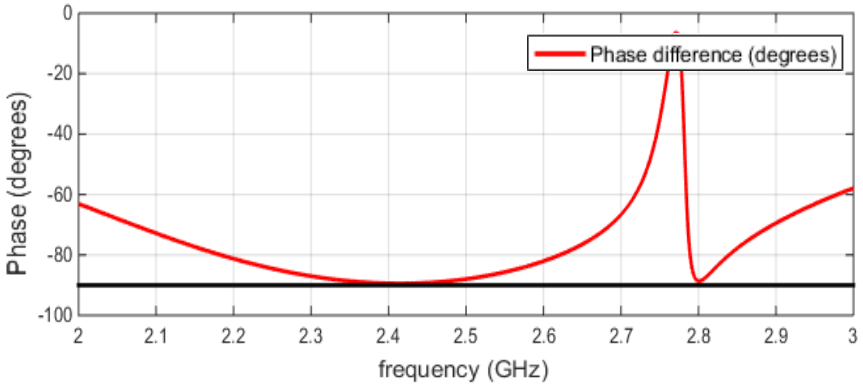

Fig. 3.2. Phase difference as a function of frequency for the nested split ring slot polarizer. The horizontal black line marks 90° phase difference.

From Fig. 3.1 and Fig. 3.2 it can be seen that the nested split slot ring polarizer generates a circularly polarized wave from a linearly polarized incident wave at 2.45 GHz.

Fig. 3.3 shows the axial ratio (in dB) across the 2 GHz to 3 GHz frequency range. The axial ratio was calculated as the ratio of the major to minor axis [2].

From Fig. 3.3 it can be seen that the simulated axial ratio is below 3 dB from 2.335 GHz to 2.56 GHz. An axial ratio bandwidth of 225 MHz, 9.18%, is achieved.

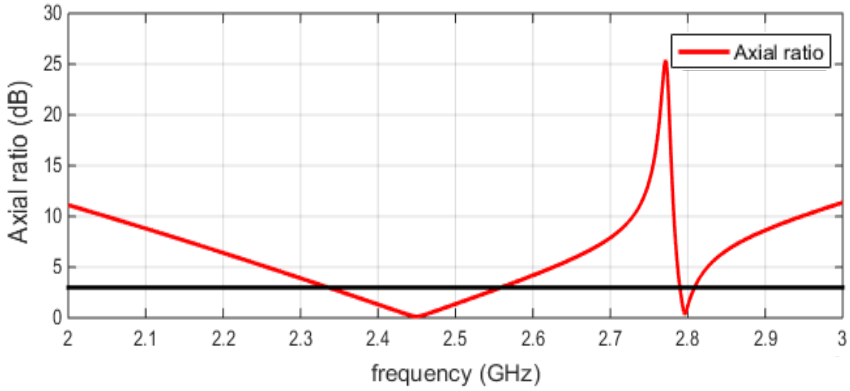

Fig. 3.3. Simulated axial ratio in dB. The horizontal black line indicates the 3dB axial ratio level.

3.2.2 Jerusalem-cross polarizer

In [2] dimensions were provided for a Jerusalem-cross unit cell which operates at a centre frequency of 17.8 GHz. To design a Jerusalem-cross unit cell which operates at 2.45 GHz, CST was used to optimize these dimensions. The dimensions were optimized for -3 dB (equal) magnitude and a phase difference of 90° between the horizontal and vertical components at 2.45 GHz. The thickness of the substrate and the substrate material was also varied.

The Jerusalem-cross unit cell is shown in Fig. 2.4. The dimensions determined for a centre frequency of 2.45 GHz are $l_1 = l_2 = 23.04$ mm, $l_3 = 34.11$ mm, $l_4 = 21.52$ mm, $w_1 = 1.62$ mm and, $w_2 = 3.65$ mm. The period of the unit cell is 41.66 mm.

Fig. 3.4 shows the simulated axial ratio, across the 2 GHz to 3 GHz frequency range.

From Fig. 3.4 it can be seen that the simulated axial ratio is below 3 dB from 2.313 GHz to 2.573 GHz. An axial ratio bandwidth of 260 MHz, 10.6%, is achieved.

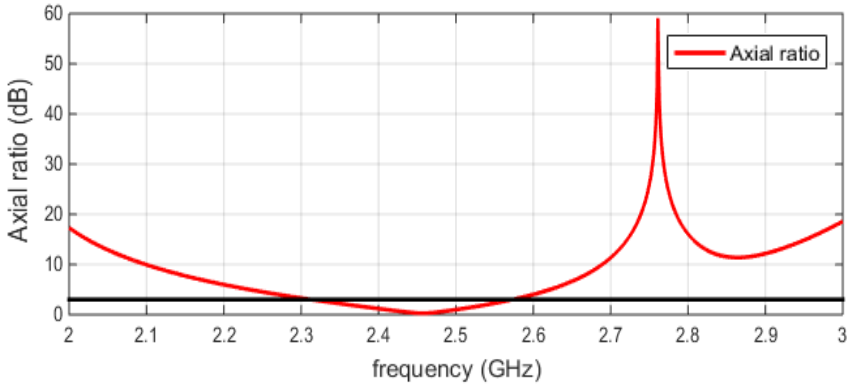

Fig. 3.4. Simulated axial ratio in dB. The horizontal black line indicates the 3dB axial ratio level.

3.2.3 Rectangular loop with a diagonal microstrip polarizer

In [7] dimensions were provided for a rectangular loop with a diagonal microstrip unit cell which operates at a centre frequency of 2.45 GHz. Since this is the desired operating frequency only a small number of iterations were required to optimize the given dimensions for a different substrate material and substrate thickness.

The rectangular loop with a diagonal microstrip unit cell is shown in Fig. 2.5. The dimensions for a centre frequency of 2.45 GHz are l = 35.98 mm, w_2 = 0.93 mm and, w_1 = 1.05 mm. The period of the unit cell is 47.06 mm.

Fig. 3.5 shows the axial ratio across the 2 GHz to 3 GHz frequency range.

From Fig. 3.5 it can be seen that the simulated axial ratio is below 3 dB from 2.33 GHz to 2.627 GHz. An axial ratio bandwidth of 297 MHz, 12.12%, is achieved.

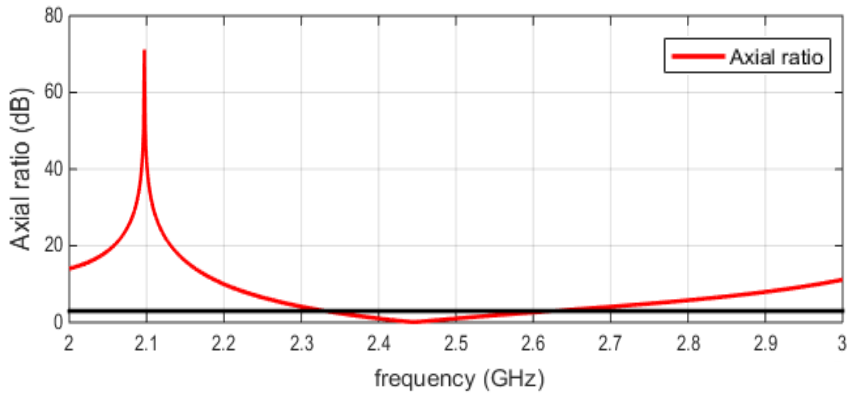

Fig. 3.5. Simulated axial ratio in dB. The horizontal black line indicates the 3dB axial ratio level.

3.2.4 Cross slot polarizer

In [8] dimensions were provided for a cross slot unit cell which operates at a centre frequency of 4.4 GHz. CST was used to optimize these dimensions, to create a cross slot unit cell which operates at 2.45 GHz. The dimensions were optimized for a phase difference of 90° between the horizontal and vertical components and -3 dB (equal) magnitude at 2.45 GHz. The thickness of the substrate and the substrate material was also altered.

The cross-slot unit cell is shown in Fig. 2.6. The dimensions determined for a centre frequency of 2.45 GHz are l_1 = 47.71 mm, l_2 = 73.6 mm and, w = 4.52 mm. The period of the unit cell is 59.18 mm.

Fig. 3.6 shows the axial ratio across the 2 GHz to 3 GHz frequency range.

From Fig. 3.6 it can be seen that the simulated axial ratio is below 3 dB from 2.319 GHz to 2.571 GHz. An axial ratio bandwidth of 252 MHz, 10.29%, is achieved.

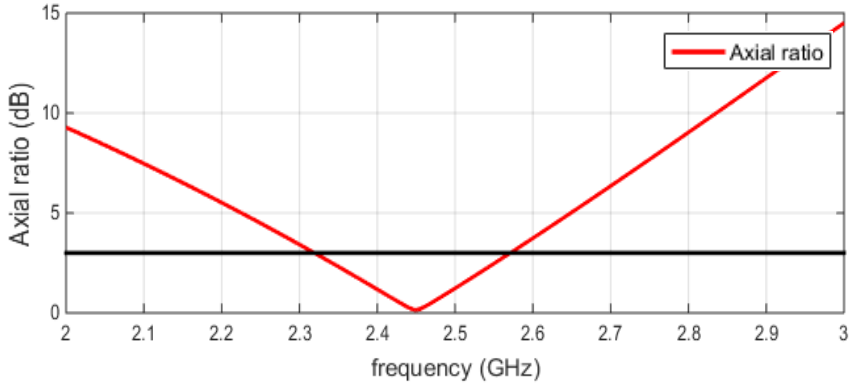

Fig. 3.6. Simulated axial ratio in dB. The horizontal black line indicates the 3dB axial ratio level.

3.2.5 Metallic ring with embedded rectangular strip polarizer

In [1] dimensions were provided for a metallic ring with embedded rectangular strip unit cell which operates at a centre frequency of 14.5 GHz. To create a metallic ring with embedded rectangular strip unit cell which operates at 2.45 GHz, CST was used to optimize these dimensions. The dimensions were optimized for -3 dB (equal) magnitude and a phase difference of 90° between the horizontal and vertical components at 2.45 GHz. The thickness of the substrate and the substrate material was also altered.

The metallic ring with embedded rectangular strip unit cell is shown in Fig. 2.7. The dimensions determined for a centre frequency of 2.45 GHz are l = 42.55 mm, w = 2.41 mm, r_1 = 23.41 mm and, r_2 = 26.70 mm. The period of the unit cell is 55.50 mm.

Fig. 3.7 shows the axial ratio across the 2 GHz to 3 GHz frequency range.

From Fig. 3.7 it can be seen that the simulated axial ratio is below 3 dB from 2.276 GHz to 2.619 GHz. An axial ratio bandwidth of 343 MHz, 14%, is achieved.

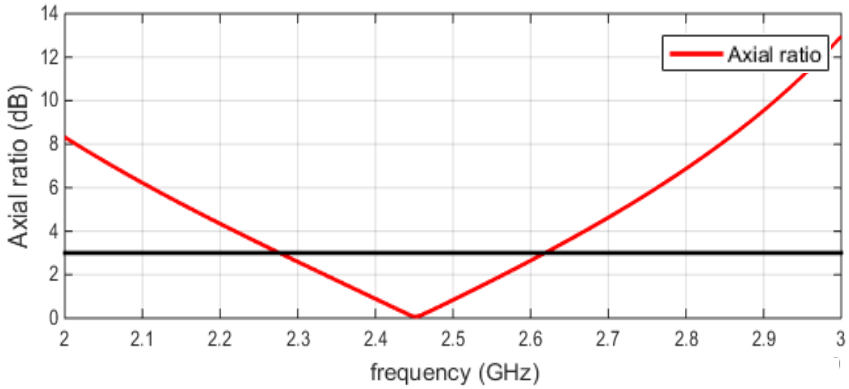

Fig. 3.7. Simulated axial ratio in dB. The horizontal black line indicates the 3dB axial ratio level.

From Fig. 3.3 to Fig. 3.7 it can be seen that the metallic ring with embedded rectangular strip polarizer has the largest axial ratio bandwidth, 14%. It can also be seen that the Jerusalem-cross polarizer has the smallest surface area of the five polarizers.

3.3 REFLECTIVE LINEAR-TO-CIRCULAR POLARIZERS

A single unit cell and the unit cell boundary condition will be used to study the performance of a reflective linear-to-circular polarizer. A 45° linearly polarized wave was chosen as the excitation. In order to achieve circular polarization, the polarizer must produce a plus 45° and minus 45° linearly polarized wave of equal magnitude with a phase difference of 90° between them, after reflection.

Only a single reflective linear-to-circular polarizer will be studied, namely the ground backed Jerusalem-cross, as this was the only single-layer reflective linear-to-circular polarizer found in the literature. The ground backed Jerusalem-cross polarizer was optimized to operate at a centre frequency of 10 GHz, for practical considerations such as the thickness of dielectric layer needed, using CST. The polarizer's dimensions and simulated axial ratio results are presented below.

3.3.1 Ground backed Jerusalem-cross polarizer

The ground backed Jerusalem-cross unit cell is shown in Fig. 2.16. The substrate material was changed from F4B to Rogers 4003C with ε_r = 3.38, tan δ = 0.0027 and thickness h = 3 mm. The dimensions determined are l_1 = l_2 = 1.56 mm, l_3 = 3.82 mm, l_4 = 4.76 mm, and w = 0.5 mm. The period of the unit cell is 6.78 mm and 7.08 mm in the horizontal and vertical directions respectively.

Fig. 3.8 shows the simulated axial ratio in dB, across the 6 GHz to 13 GHz frequency range. Axial ratio was calculated as the ratio of the major to minor axis [2].

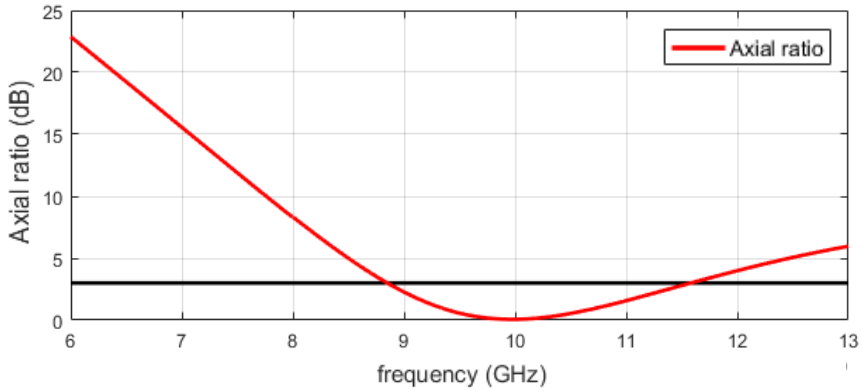

Fig. 3.8. Simulated axial ratio in dB. The horizontal black line indicates the 3dB axial ratio level.

From Fig. 3.8 it can be seen that the axial ratio is below 3 dB from 8.85 GHz to 11.58 GHz. An axial ratio bandwidth (ARBW) of 2.73 GHz, 26.73% is achieved.

3.4 CHAPTER SUMMARY

In this chapter the performance of five linear-to-circular transmission polarizers and one reflective linear-to-circular polarizer were studied.

In order to facilitate a meaningful comparison between the five linear-to-circular transmission polarizers, these polarizers were redesigned to operate at the same frequency,

2.45 GHz, and implemented on the same substrate. When comparing the five linear-to-circular transmission polarizers it was found that the Jerusalem-cross polarizer has the smallest unit cell and the nested split ring slot polarizer has the largest unit cell. It was also found that the metallic ring with embedded rectangular strip polarizer has the largest axial ratio bandwidth, 14%, and that the nested split ring slot polarizer has the smallest axial ratio bandwidth, 9.8%, of the five polarizers.

The reflective linear-to-circular polarizer achieves an axial ratio bandwidth of 26.73%, and has a small unit cell.

It can be concluded that the geometry of the unit cell does have an influence on the axial ratio bandwidth of the unit cell. The aim is to find a new unit cell or optimize an existing unit cell for improved axial ratio bandwidth.

CHAPTER 4 TRANSMISSION POLARIZER DESIGN PROCEDURE

4.1 CHAPTER OVERVIEW

This chapter focuses on the design of a thin single-layer linear-to-circular transmission polarizer with enhanced bandwidth. The starting point was a conventional Jerusalem-Cross geometry [2]. In Section 4.2 results of a parametric study on the Jerusalem-cross unit cell are presented. In Section 4.3 an equivalent circuit model is presented that gives some insight in the performance of the Jerusalem-cross array. In Section 4.4 a new unit cell geometry is derived using the knowledge gained from the equivalent circuit model and the parametric study. In Section 4.5 the simulation results of the new unit element are presented and a numerical experiment is discussed.

4.2 PARAMETRIC STUDY

A parametric study was performed on a scaled version of the Jerusalem-cross polarizer presented in [2], to determine whether an improvement in axial ratio bandwidth could be achieved. For ease of reference the geometry of the unit cell is repeated in Fig. 4.1, with some of the dimensions shown in the figure.

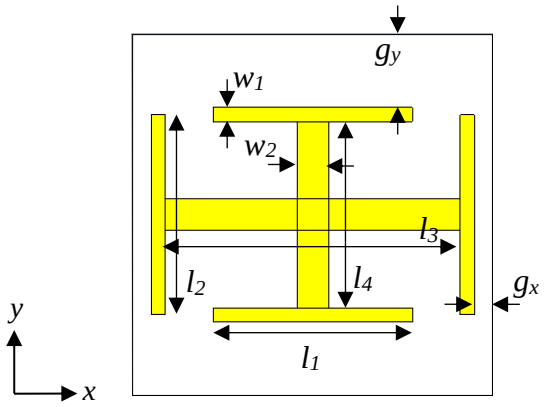

Fig. 4.1. Jerusalem-cross unit cell [2].

4.2.1 Simulation of unit cell

The unit cell was excited with a 45° linearly polarized wave, which is the superposition of a vertical (E_{v0}^{i}) and horizontal (E_{h0}^{i}) polarized wave of equal magnitude and phase. The magnitudes of the transmitted electric fields $|E_h^t|$ and $|E_v^t|$ are given by (4.1) and (4.2), where the transmission coefficients for the vertical and horizontal polarizations are defined as T_v and T_h respectively

$$\left|E_h{}^t\right| = T_h\left|E_{h0}{}^i\right|, \tag{4.1}$$

$$\left|E_v{}^t\right| = T_v\left|E_{v0}{}^i\right|. \tag{4.2}$$

The phase difference between the transmitted electric fields can be calculated using (4.3)

$$\angle E_h{}^t - \angle E_v{}^t = \angle T_h - \angle T_v = \phi. \tag{4.3}$$

In order to achieve circular polarization, the polarizer must enforce a 90° phase difference ($\angle T_h - \angle T_v = 90°$) and equal magnitude ($|T_h| = |T_v|$) on the transmitted vertical (E_v^t) and horizontal (E_h^t) components.

4.2.2 Parameter Sweep

The following parameters were independently sweeped: the length of the cross sides (l_1 and l_2), and spacing to the edge of the unit cell (g_x and g_y). For each sweep performed, the value of each dimension is given in Table 4.1. The dimensions of the reference design performed in Chapter 3 are also noted.

Table 4.1 Sweeps performed.

	l_1 **(mm)**	l_2 **(mm)**	l_3 **(mm)**	l_4 **(mm)**	w_1 **(mm)**	w_2 **(mm)**	g_x **(mm)**	g_y **(mm)**
Reference design	23.04	23.04	34.11	21.52	1.62	3.65	2.16	8.45
Sweep 1	23.04	23.04	34.11	21.52	1.62	3.65	**2 - 10**	8.45
Sweep 2	23.04	23.04	34.11	21.52	1.62	3.65	2.16	**2 - 10**
Sweep 3	**20 - 24**	23.04	34.11	21.52	1.62	3.65	2.16	8.45
Sweep 4	23.04	**20 - 24**	34.11	21.52	1.62	3.65	2.16	8.45

4.2.3 Parameter Sweep Results

Fig. 4.2 shows the transmission magnitude of the vertical and horizontal components across the 1 GHz to 4 GHz frequency range of the reference design.

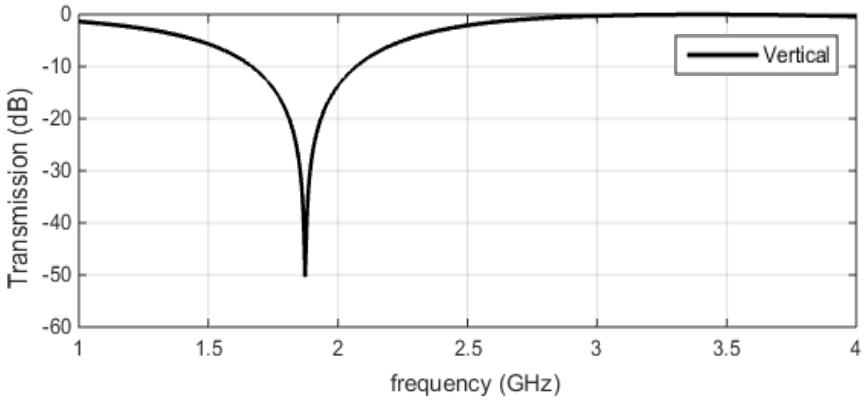

(a)

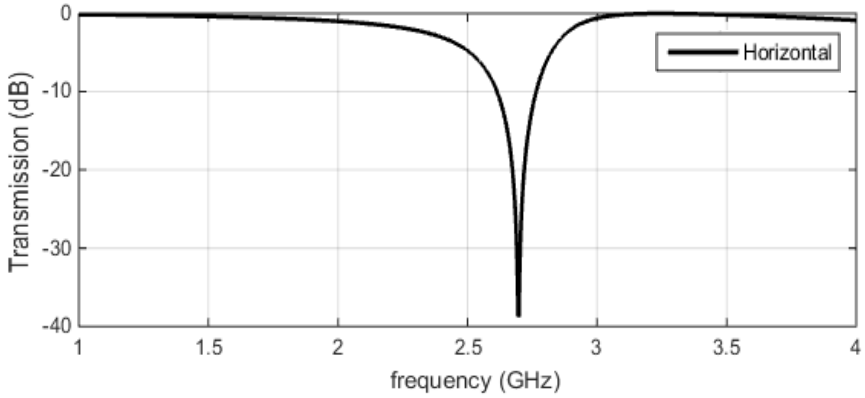

(b)

Fig. 4.2. Transmission magnitude as a function of frequency**.**

(a) Vertical component. (b) Horizontal component.

Fig. 4.3 shows the transmission magnitude of the vertical and horizontal components across the 1 GHz to 4 GHz frequency range, for sweep 1 where g_x was varied from 2 to 10 mm.

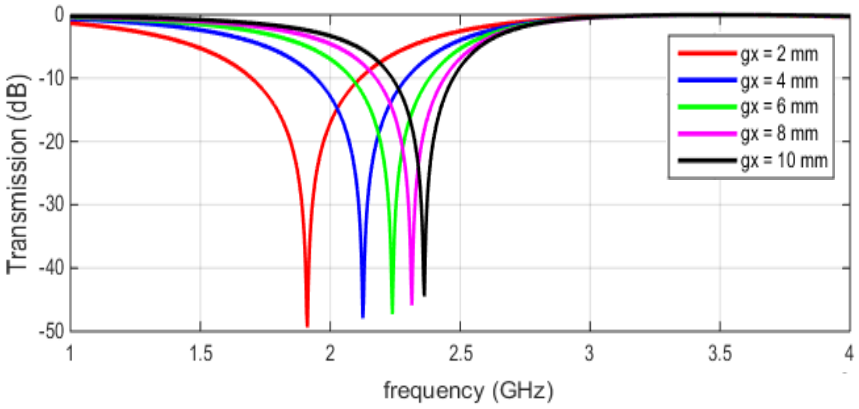

(a)

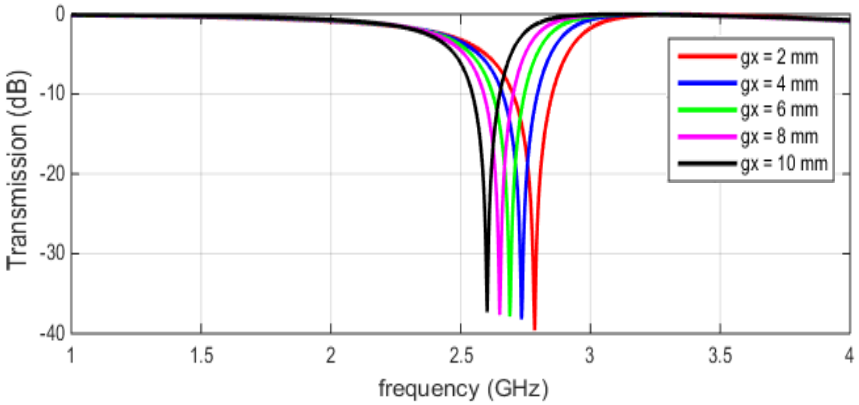

(b)

Fig. 4.3. Transmission magnitude as a function of frequency for different values of g_x (sweep 1).

(a) Vertical component. (b) Horizontal component.

Fig. 4.4 shows the transmission magnitude of the vertical and horizontal components in dB for sweep 2, where g_y was varied from 2 to10 mm, across the 1 GHz to 4 GHz frequency range.

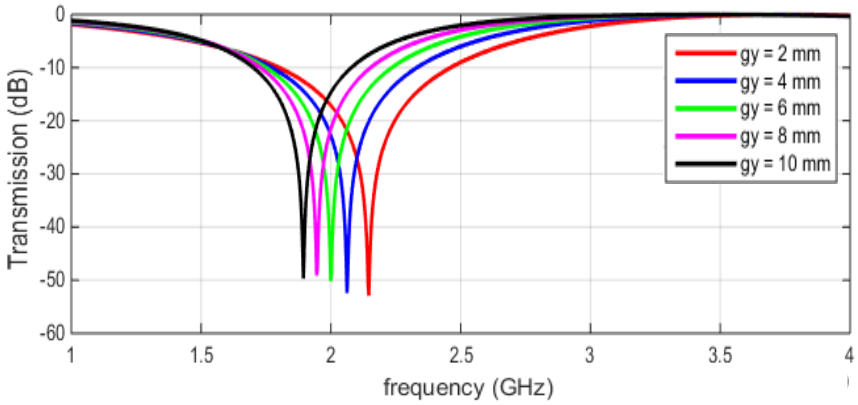

(a)

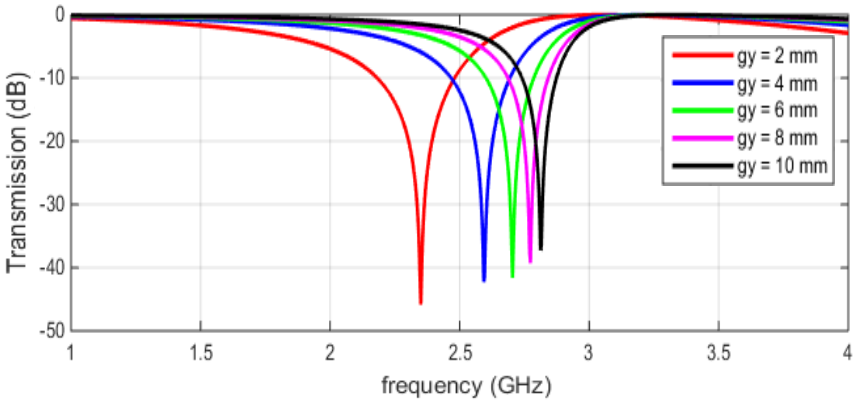

(b)

Fig. 4.4. Transmission magnitude as a function of frequency for different values of g_y (sweep 2).

(a) Vertical component. (b) Horizontal component.

It can be seen from sweep 1 that if g_x decreases the resonant frequency of the vertical component moves down in frequency (left), and as g_x increases the resonant frequency of the vertical component moves up in frequency (right). It can also be seen that g_x has an effect on the resonant frequency of the horizontal component as g_x increases the resonant frequency of the horizontal component moves down in frequency (left), and as g_x decreases the resonant frequency of the horizontal component moves up in frequency (right). From sweep 2 it can be seen that g_y has the opposite effect on the vertical and horizontal components than g_x.

Fig. 4.5 shows the transmission magnitude of the vertical and horizontal components in dB for sweep 3, where l_1 was varied from 20 to 24 mm, across the 1 GHz to 4 GHz frequency range.

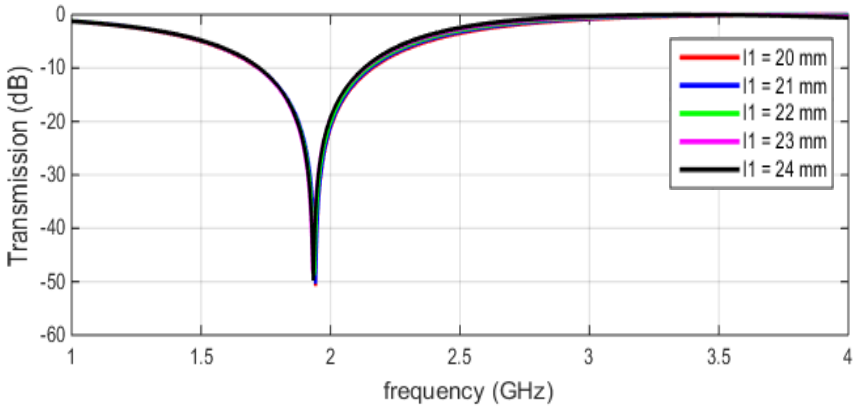

(a)

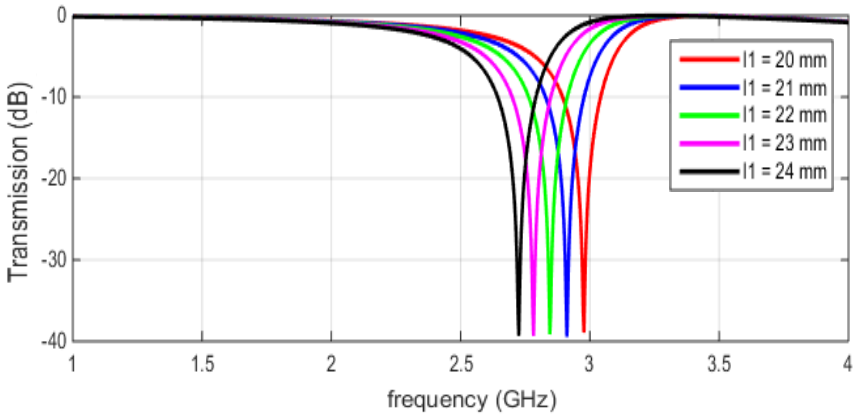

(b)

Fig. 4.5. Transmission magnitude as a function of frequency for different values of l_1 (sweep 3).

(a) Vertical component. (b) Horizontal component.

Fig. 4.6 shows the transmission magnitude of the vertical and horizontal components in dB for sweep 4, where l_2 was varied from 20 to 24 mm, across the 1 GHz to 4 GHz frequency range.

It can be seen from sweep 3 that as l_1 decreases the resonant frequency of the horizontal component moves up in frequency (right), and as l_1 increases the resonant frequency of the

horizontal component moves down in frequency (left). It can also be seen that l_1 has almost no influence on the resonant frequency of the vertical component. From sweep 4 it can be seen that l_2 has the opposite effect on the vertical and horizontal components than l_1.

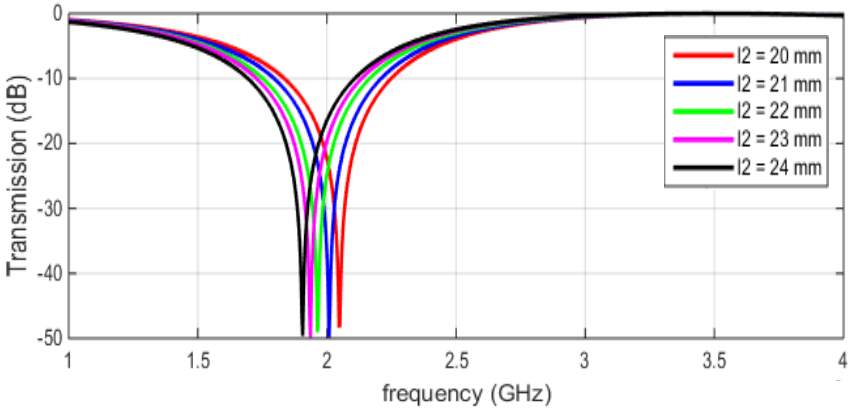

(a)

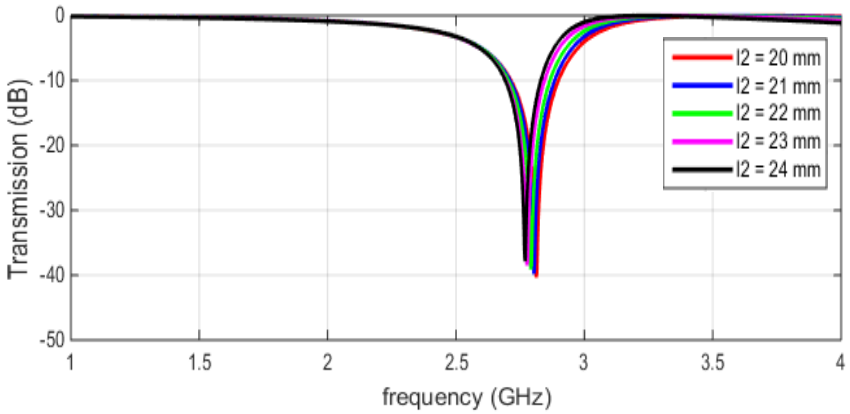

(b)

Fig. 4.6. Transmission magnitude as a function of frequency for different values of l_2 (sweep 4).

(a) Vertical component. (b) Horizontal component.

From sweep 1 to sweep 4 and Fig. 4.3 to Fig. 4.6 it can be concluded that by moving the resonant frequency of the vertical component down (left) and moving the resonant frequency of the horizontal component up (right) the -3 dB equal power split point can be controlled, and the axial ratio bandwidth can be increased. To achieve this g_x and l_1 should be as small as possible and g_y and l_2 should be as large as possible, according to the results of the parameter study.

4.3 EQUIVALENT CIRCUIT MODEL

An array can be modelled by an equivalent circuit, where the grid is represented by shunt lumped circuit impedance elements using a transmission line approach. Assume we have an array of perfectly conducting narrow strips which are thin, infinitely long and continuous. Depending on whether the incident wave is polarized parallel to or perpendicular to the edges of the strips the shunt impedance is either inductive or capacitive, respectively. For an electric field vector parallel to the strips, the inductive reactance, normalized to the impedance of free space, is given by [21]

$$X(w) = F(p, w, \lambda)$$

$$= \frac{p}{\lambda}\cos\theta\left\{\ln\left(\csc\frac{\pi w}{2p}\right) + G(p, w, \lambda)\right\}, \tag{4.4}$$

where p is the period of the array, the strips have a width w, θ is the angle of incidence, λ is the wavelength and $G(p, w, \lambda)$ is given by

$$G(p, w, \lambda) = \frac{1}{2} \times \frac{(1-\beta^2)^2\left\{\left(1-\frac{\beta^4}{4}\right)(A_+ + A_-) + 4\beta^2 A_+ A_-\right\}}{\left(1-\frac{\beta^2}{4}\right) + \beta^2\left(1+\frac{\beta^2}{2}-\frac{\beta^4}{8}\right)(A_+ + A_-) + 2\beta^6 A_+ A_-}. \tag{4.5}$$

$A_\pm$ is given by (4.6) and β is given by (4.7)

$$A_\pm = \frac{1}{\sqrt{\left(1 \pm \frac{2p\sin\theta}{\lambda} - \left(\frac{p\cos\theta}{\lambda}\right)^2\right)}} - 1 \tag{4.6}$$

$$\beta = \sin\left(\frac{\pi w}{2p}\right). \tag{4.7}$$

For an electric field vector perpendicular to the strips, the capacitive susceptance, normalized to the admittance of free space, is given by

$$B(g) = 4F(p, g, \lambda), \tag{4.8}$$

where g is the distance between the strips.

Combinations of these terms can be used to describe complex structures. The voltage reflection coefficient ρ can be determined using the complex admittance Y of the grid, as shown in (4.9). The transmission coefficient τ can be determined using the reflection coefficient, as shown in (4.10). When using this model the assumption is made that $p(1+sin\theta) < \lambda$, $w << p < \lambda$ and $g << \lambda$

$$|\rho|^2 = \frac{Y^2}{Y^2+4} \tag{4.9}$$

$$|\tau|^2 = 1 - |\rho|^2. \tag{4.10}$$

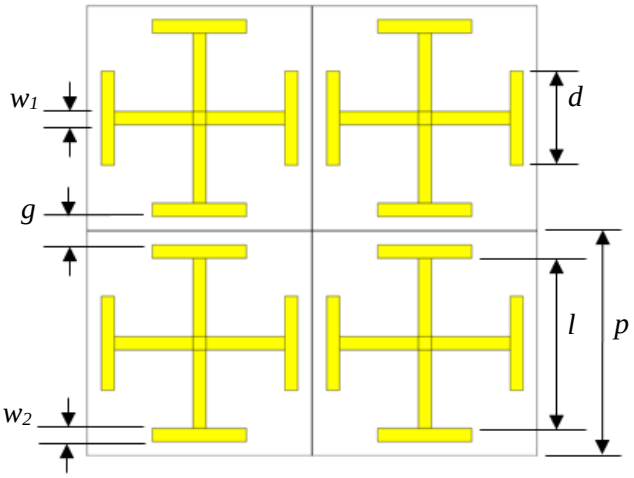

Fig. 4.7. Jerusalem-cross array.

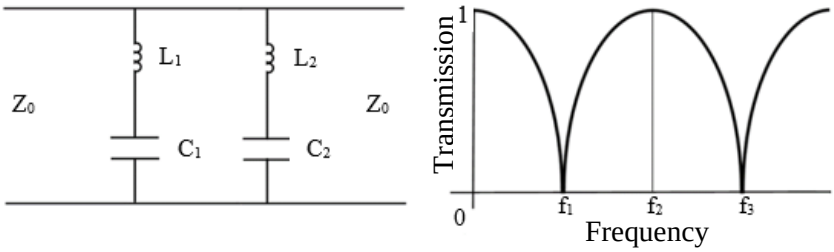

(a) (b)

Fig. 4.8. Equivalent circuit model [21].

(a) Equivalent circuit. (b) Frequency response.

An equivalent circuit, which consists of two resonant series LC circuits in parallel, can be used to model the transmission of a vertically or horizontally polarized plane wave (normally incident) through a planar Jerusalem-cross array shown in Fig. 4.7 [21]. The equivalent circuit and its frequency response (magnitude of the transmission coefficient) is shown in Fig. 4.8. L_1 is accounted for by the inductive strips of width w_1 and can be calculated using (4.4). The capacitance between the horizontal end capacitors, spaced g apart, is given by

$$B_g = \frac{4d}{p} F(p, g, \lambda). \tag{4.11}$$

The capacitance between the vertical end capacitors, spaced (p-d) apart, is given by

$$B_d = \frac{4(2*w_2+g)}{p} F(p, p-d, \lambda). \tag{4.12}$$

The susceptance B_g and B_d combine to form the susceptance B_1 of the capacitance C_1.

L_2 and C_2 can be calculated using a different approach. By using the assumption of a dipole resonance at f_3, the resonant wavelength can be calculated as $\lambda_3 = d/0.43$. Using the series resonant circuit equation, given by (4.13), L_2 and C_2 can be calculated. L_1 and C_1 can also be calculated in a similar manner [21].

$$f_3 = \frac{1}{2\pi\sqrt{L_2 C_2}} \tag{4.13}$$

From (4.13) it can be seen that by altering the dimensions of the two I-shaped structures which form the Jerusalem-cross, the capacitance and inductance of the two series resonant circuits, and hence the position of the transmission zeros, can be controlled. The aim is to adjust the locations of the pairs of resonances (one pair for horizontal polarization, one pair for vertical polarization) to increase the frequency range across which equal power transmission, and a 90° phase difference is achieved and as such increase the circular polarization axial ratio bandwidth.

4.4 UNIT CELL DERIVATION

A new unit cell was designed with the knowledge gained from the parametric analysis and the equivalent circuit model (small g_x and l_1 and large g_y and l_2). CST Microwave Studio was used as simulation tool and optimization of all parameters (including l_3 and l_4) was performed to determine the dimensions of the new unit cell for operation at 2.45 GHz. Consider the symmetric Jerusalem-cross unit cell shown in Fig. 4.9 (a). The symmetric Jerusalem-cross unit cell was designed to have, for both the horizontal and vertical components of a 45° incident wave, a resonant frequency of 2.45 GHz, as shown in Fig. 4.10 (a). The resonant frequency of the vertical component, can be moved down in frequency, by increasing the coupling between adjacent unit cells for the vertical I-shape, as shown in Fig. 4.9 (b) and Fig. 4.10 (b). This, however, resulted in unrealizable coupling gap dimensions. To maintain the increase in coupling between adjacent cells and obtain realizable coupling gap dimensions between adjacent cells, extra capacitive strips are etched on the back of the substrate, as shown in red in Fig. 4.9 (c) and Fig. 4.10 (c). The resonant frequency of the horizontal component can be moved up in frequency, by reducing the coupling of the horizontal I-shape, as shown in Fig. 4.9 (d) and Fig. 4.10 (d). From Fig. 4.10 (a) to Fig. 4.10 (d) it can be seen that the two pairs of resonances can be controlled almost independently.

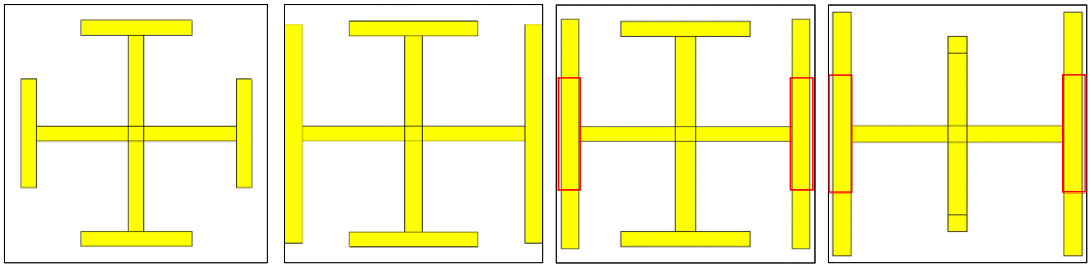

(a) (b) (c) (d)

Fig. 4.9. Derivation of new unit cell.

(a) Symmetric Jerusalem-cross unit cell. (b) Unit cell after horizontal dipole modification. (c) Unit cell after horizontal dipole modification with realizable coupling gap dimensions, capacitive strips etched on the back is shown in red. (d) Unit cell after both vertical and horizontal dipole modification.

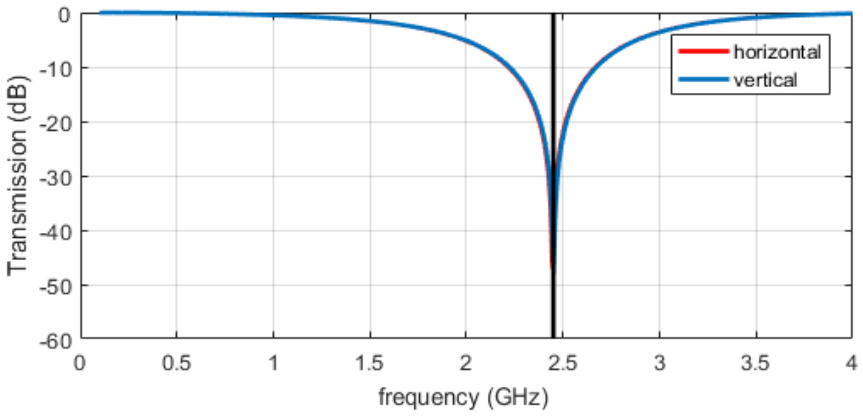

(a)

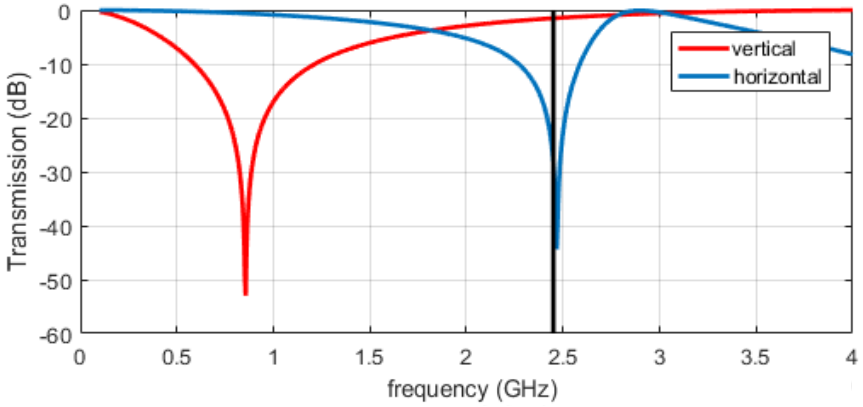

(b)

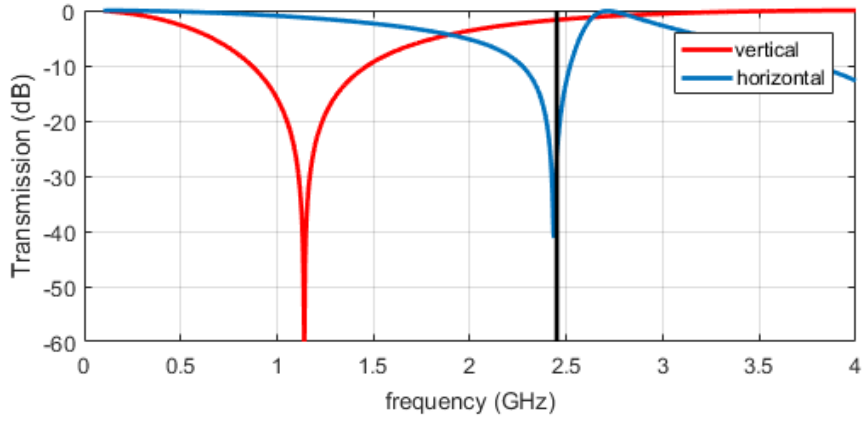

(c)

Fig. 4.10. Adjustment of the location of transmission zeros.

Symmetric Jerusalem-cross frequency response. (b) Frequency response after horizontal dipole modification. (c) Frequency response after horizontal dipole modification with realizable coupling gap dimensions.

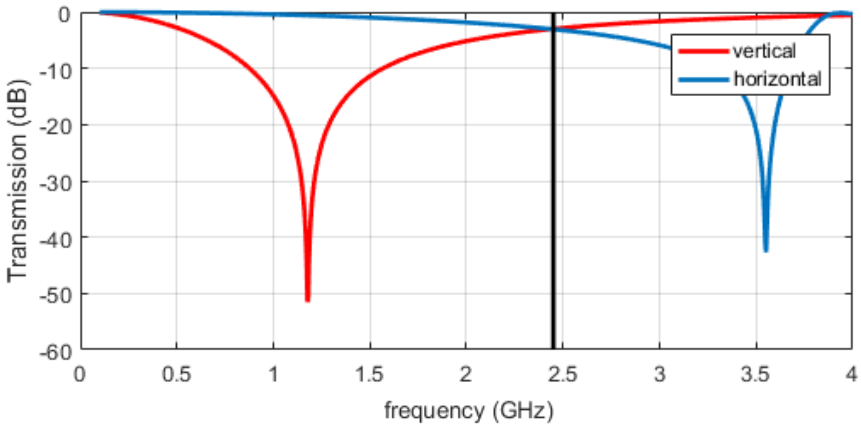

(d)

Fig. 4.10. (Continued) Adjustment of the location of transmission zeros.

(d) Frequency response after both vertical and horizontal dipole modification.

4.5 CST SIMULATION

4.5.1 CST model of proposed unit cell

The proposed unit cell is shown in Fig. 4.11.

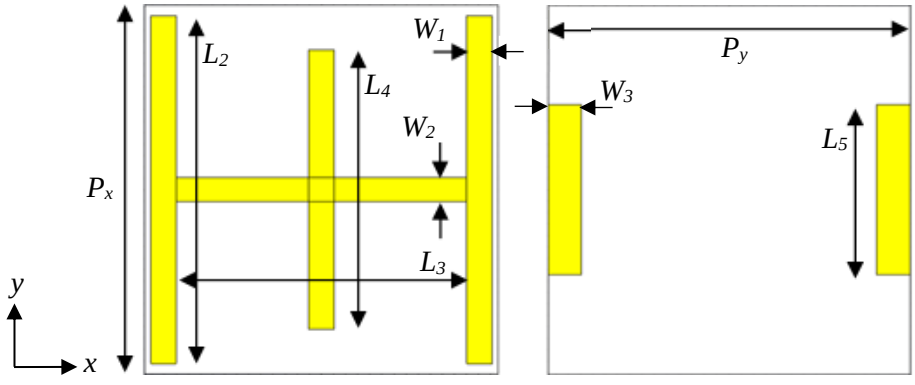

(a) (b)

Fig. 4.11. Proposed unit cell.

(a) Front view. (b) Back view.

The substrate material is Rogers 4003C with εr = 3.38, tan δ = 0.0027 and thickness h = 0.813 mm. The dimensions are P_x = 32.3 mm, P_y = 29.2 mm, L_2 = 30.5 mm, L_3 = 24 mm, L_4 = 24.5 mm, L_5 = 14.9 mm and, W_1 = W_2 = W_3 = 2.1 mm.

4.5.2 Simulation results of proposed unit cell

To verify the performance of the proposed polarizer, full wave simulations were conducted using CST.

4.5.2.1 Transmission magnitude

Fig. 4.12 shows the simulated transmission magnitude of the horizontal and vertical components in dB, across the 1.5 GHz to 3.5 GHz frequency range.

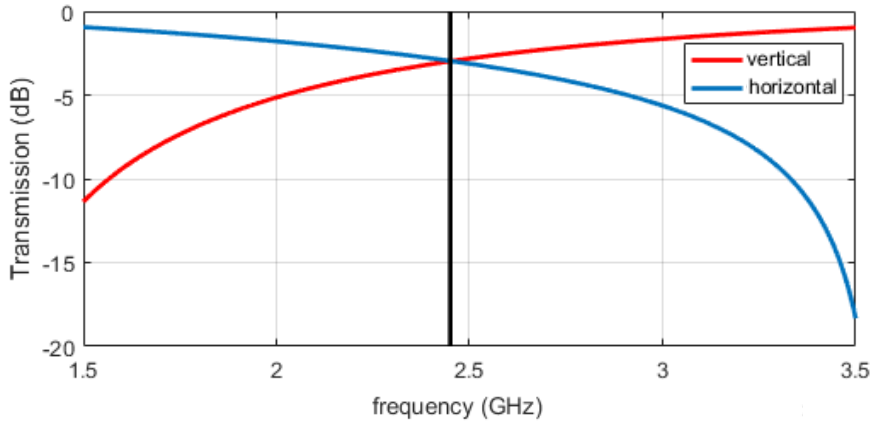

Fig. 4.12. Simulated magnitude of the transmission coefficients of the vertical and horizontal components. The vertical black line indicates the 2.45 GHz point where equal magnitude is required (-3 dB).

It can be seen from Fig. 4.12 that the point of equal magnitude and equal power transmission is about 2.45 GHz for the proposed polarizer.

4.5.2.2 Phase difference

Fig. 4.13 shows the phase difference between the horizontal and vertical components, across the 1.5 GHz to 3.5 GHz frequency range.

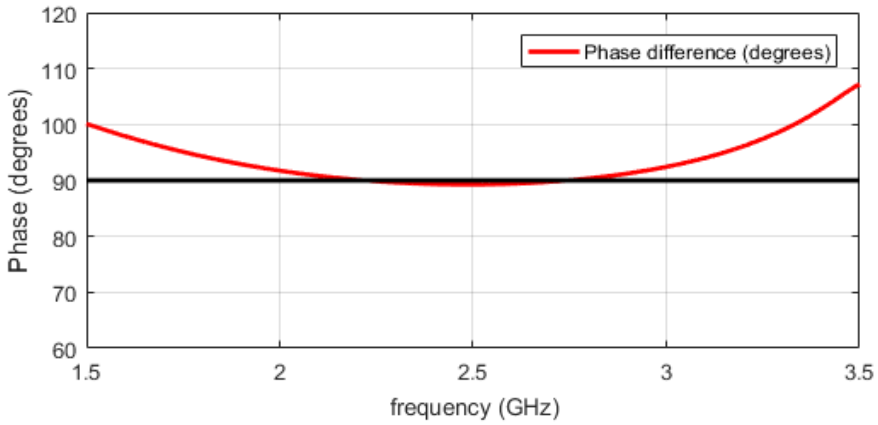

Fig. 4.13. Simulated phase difference between the vertical and horizontal components. The horizontal black line marks 90° phase difference level.

It can be seen from Fig. 4.13 that the phase difference is approximately 90° at 2.45 GHz for the proposed polarizer.

4.5.2.3 Axial ratio

The axial ratio was calculated as the ratio of the major to minor axis, using (4.14) where ϕ is the phase difference between the transmitted electric fields [2]

$$AR = 20\log_{10}\left[\frac{\sqrt{\frac{1}{2}\left(|E_h{}^t|^2+|E_v{}^t|^2+\sqrt{|E_h{}^t|^4+|E_v{}^t|^4+2\left(|E_h{}^t|^2|E_v{}^t|^2\cos 2\phi\right)}\right)}}{\sqrt{\frac{1}{2}\left(|E_h{}^t|^2+|E_v{}^t|^2-\sqrt{|E_h{}^t|^4+|E_v{}^t|^4+2\left(|E_h{}^t|^2|E_v{}^t|^2\cos 2\phi\right)}\right)}}\right]. \quad (4.14)$$

Fig. 4.14 shows the axial ratio, across the 1.5 GHz to 3.5 GHz frequency range.

It can be seen from Fig. 4.14 that the axial ratio is below 3 dB across the 2.036 GHz to 2.877 GHz frequency range.

4.5.2.4 Discussion

It can be seen from Fig. 4.12 and Fig. 4.13 that the proposed polarizer produces a 90° phase difference between the horizontal and vertical components, of the incident wave, while maintaining equal magnitude at 2.45 GHz, almost perfect circular polarization is obtained at 2.45 GHz. From Fig. 4.14 it can be seen that the proposed polarizer achieves a 3 dB axial ratio bandwidth of 34%.

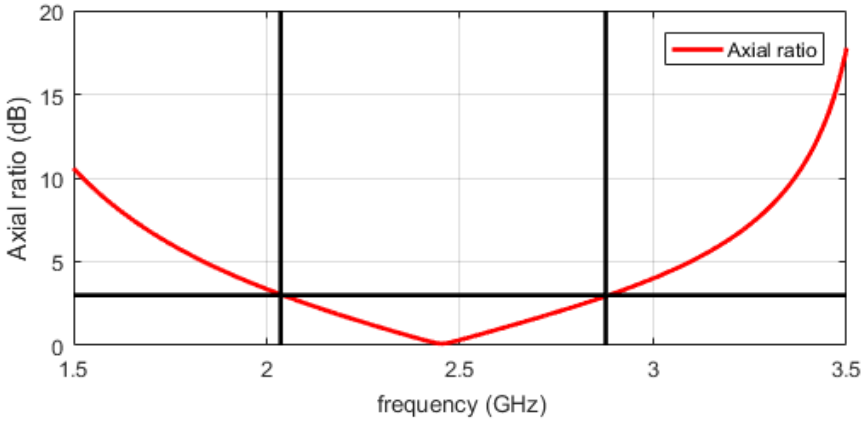

Fig. 4.14. Simulated axial ratio. The horizontal black line indicates the 3dB axial ratio level. The two vertical black lines represents the 3 dB axial ratio bandwidth.

4.5.3 Description of numerical experiment

All the unit cells analyzed so far, were simulated using the unit cell boundary condition which duplicates the unit cell in the *X*-*Y* plane of the global coordinate system an infinite number of times. The results obtained for these unit cells are then for the ideal case, an infinite FSS. In this section a numerical experiment is performed to determine whether a finite sized polarizer's performance is satisfactory.

A scaled version of the Jerusalem-cross polarizer presented in [2] is used for the numerical experiment. An FSS polarizer was created which consists of a 100 identical Jerusalem-cross unit cells in a 10 x 10 configuration.

The top view of the Jerusalem-cross FSS polarizer is shown in Fig. 4.15.

CST microwave Studio was used to perform the numerical experiment. Plane wave excitation was used to excite the 10 x 10 polarizer on a specified side and probes were used on the other side to measure the resulting electric fields. The polarizer was excited by a 45° linearly polarized plane wave, which consists of the superposition of a vertical and horizontal polarized wave with equal magnitudes and phase. In order to achieve circular polarization,

the polarizer must produce a 90° phase difference between the vertical and horizontal components without changing the magnitudes.

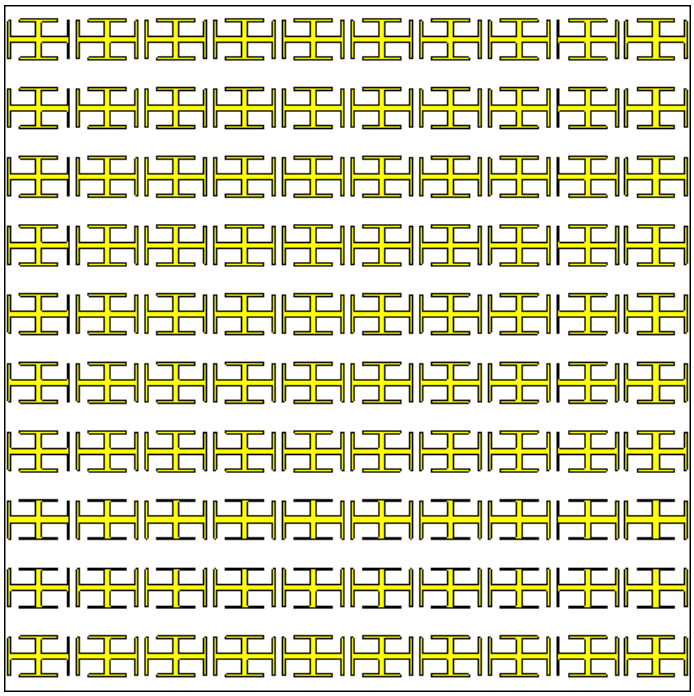

Fig. 4.15. Jerusalem-cross FSS polarizer.

The 10 x 10 Jerusalem-cross FSS polarizer's CST simulation results are compared to the scaled Jerusalem-cross (infinite FSS) CST simulation results below.

4.5.4 Magnitude results

4.5.4.1 Infinite Jerusalem-cross FSS polarizer

Fig. 4.16 shows the transmission magnitude of the vertical and horizontal components of the scaled Jerusalem-cross polarizer, across the 2 GHz to 3 GHz frequency range.

It can be seen from Fig. 4.16 that the point of equal magnitude and equal power transmission is approximately 2.45 GHz.

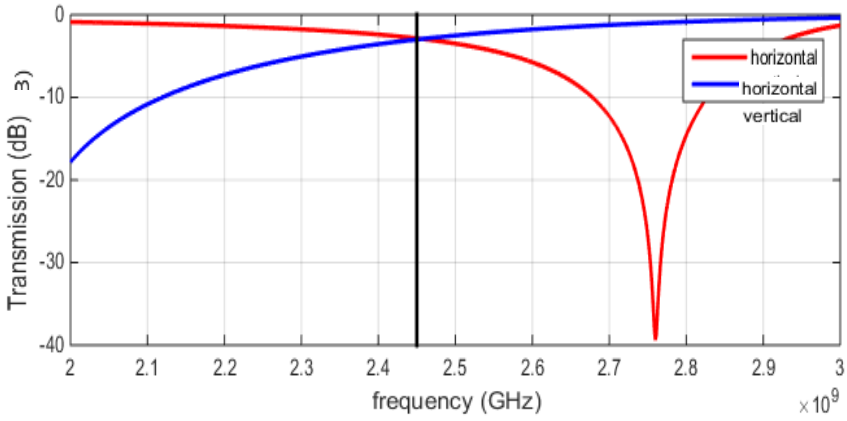

Fig. 4.16. Transmission magnitude as a function of frequency for the scaled Jerusalem-cross polarizer. The vertical black line indicates the 2.45 GHz point where equal magnitude is required (-3 dB).

4.5.4.2 10 x 10 Jerusalem-cross FSS polarizer

Fig. 4.17 shows the transmission magnitude of the vertical and horizontal components, across the 2 GHz to 3 GHz frequency range, for the 10 x 10 Jerusalem-cross FSS polarizer. It can be seen from Fig. 4.17 that the point of equal magnitude and equal power transmission is approximately 2.58 GHz.

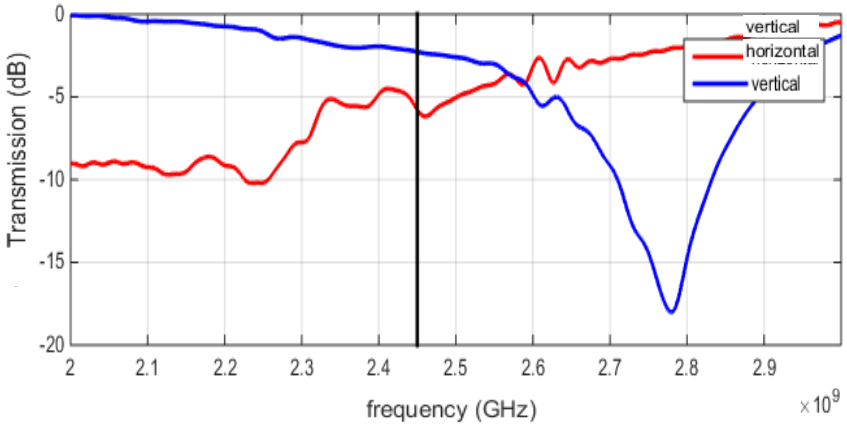

Fig. 4.17. Transmission magnitude as a function of frequency for the 10 x 10 Jerusalem-cross FSS polarizer. The vertical black line indicates the 2.45 GHz point where equal magnitude is required (-3 dB).

4.5.5 Phase results

4.5.5.1 Infinite Jerusalem-cross FSS polarizer

Fig. 4.18 shows the phase difference between the vertical and horizontal components of the scaled Jerusalem-cross polarizer, across the 2 GHz to 3 GHz frequency range.

It can be seen from Fig. 4.18 that the phase difference is approximately 90° at 2.45 GHz.

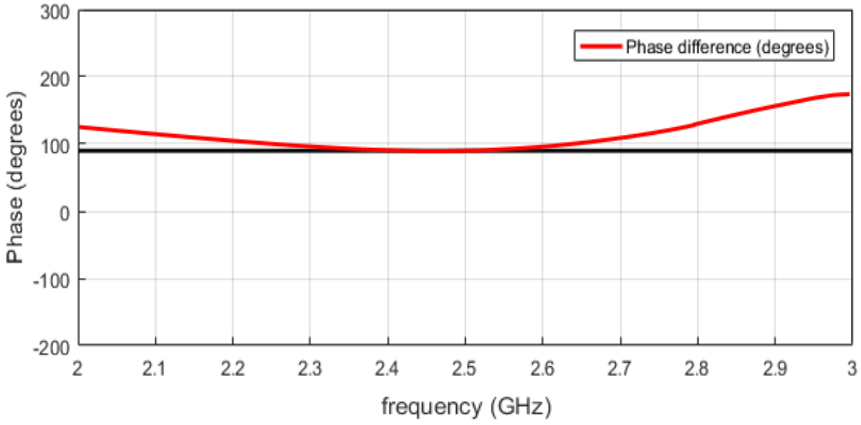

Fig. 4.18. Phase difference as a function of frequency for the scaled Jerusalem-cross polarizer. The horizontal black line marks 90° phase difference.

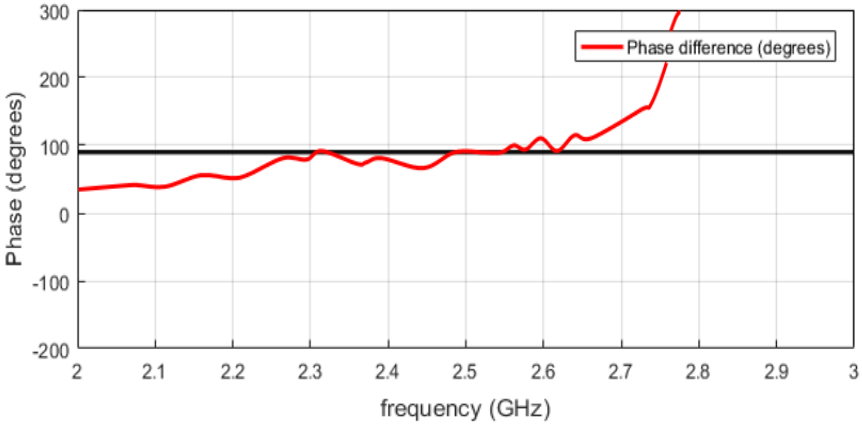

Fig. 4.19. Phase difference as a function of frequency for the 10 x 10 Jerusalem-cross FSS polarizer. The horizontal black lines marks 90° phase difference.

4.5.5.2 10 x 10 Jerusalem-cross FSS polarizer

Fig. 4.19 shows the phase difference between the vertical and horizontal components of the 10 x 10 Jerusalem-cross FSS polarizer, across the 2 GHz to 3 GHz frequency range.

It can be seen from Fig. 4.19 that that the phase difference is approximately 70° at 2.45 GHz.

4.5.6 Axial ratio results

4.5.6.1 Infinite Jerusalem-cross FSS polarizer

Fig. 4.20 shows the axial ratio of the scaled Jerusalem-cross polarizer, across the 2 GHz to 3 GHz frequency range. Axial ratio was calculated as the ratio of the major to minor axis [2]. It can be seen from Fig. 4.20 that the axial ratio is below 3 dB across the 2.313 GHz to 2.573 GHz frequency range. An axial ratio bandwidth of 260 MHz, 10.6%, is achieved.

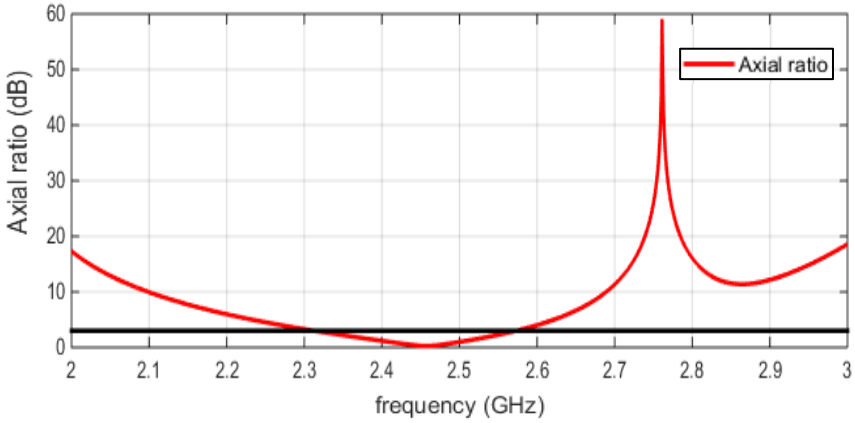

Fig. 4.20. Axial ratio as a function of frequency for the scaled Jerusalem-cross polarizer. The horizontal black line represents the 3 dB axial ratio level.

4.5.6.2 10 x 10 Jerusalem-cross FSS polarizer

Fig. 4.21 shows the axial ratio of the 10 x 10 Jerusalem-cross FSS polarizer, across the 2 GHz to 3 GHz frequency range. Axial ratio was also calculated as the ratio of the major to minor axis [2]. It can be seen from Fig. 4.21 that the axial ratio is below 3 dB across the 2.48 GHz to 2.63 GHz frequency range. An axial ratio bandwidth of 61 MHz, 6%, is achieved.

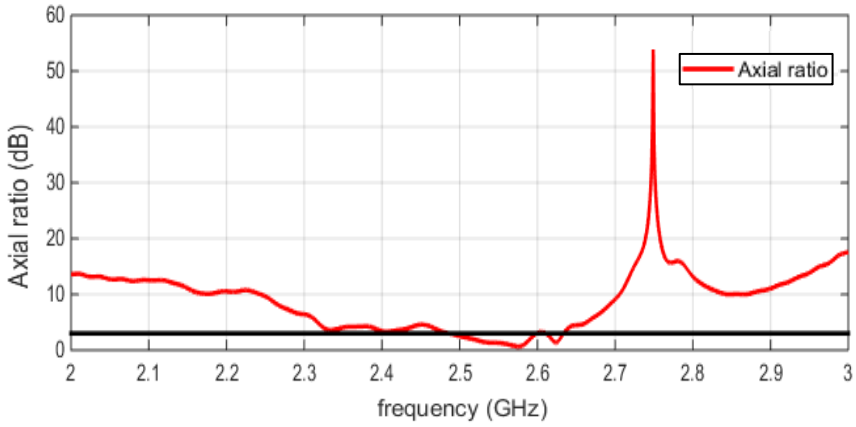

Fig. 4.21. Axial ratio as a function of frequency for the 10 x 10 Jerusalem-cross FSS polarizer. The horizontal black line represents the 3 dB axial ratio level.

4.6 DISCUSSION AND CONCLUSION

From Fig. 4.16 and Fig. 4.17 it can be seen that the transmission amplitude of the vertical and horizontal components of the 10 x 10 Jerusalem-cross FSS polarizer has a similar shape to the transmission amplitude of the infinite Jerusalem-cross polarizer. Fig. 4.17 is a fair approximation of Fig. 4.16. From Fig. 4.18 and Fig. 4.19 it is seen that both phase differences are close to 90° in the 2.2 GHz to 2.7 GHz range. From Fig. 4.20 and Fig. 4.21 it can be seen that the axial ratio of the 10 x 10 Jerusalem-cross FSS polarizer has a similar shape to the axial ratio of the scaled Jerusalem-cross polarizer. Fig. 4.21 is a fair approximation of Fig. 4.20.

The results differ because of the different number of mesh elements used in each simulation. The mesh influences the accuracy of the simulation and the simulation time. The more mesh elements used the better the accuracy. Fig. 4.22 shows the mesh used to simulate the infinite Jerusalem-cross and Fig. 4.23 shows the mesh used to simulate the 10 x 10 Jerusalem-cross FSS polarizer. When comparing these two figures it can be seen that the mesh used to simulate the scaled Jerusalem-cross is much finer, and as such also more accurate, than the one used to simulate the 10 x 10 Jerusalem-cross FSS polarizer. The mesh used to simulate the 10 x 10 Jerusalem-cross FSS polarizer could also be made finer, but then computer

memory becomes a problem. To simulate the 10 x 10 Jerusalem-cross FSS polarizer with the same accuracy used to simulate the scaled Jerusalem-cross, about 400 GB RAM would be required. It is not viable to simulate a finite structure with multiple unit elements.

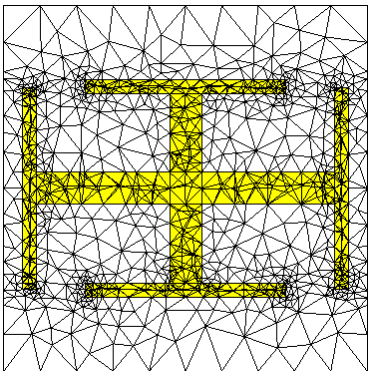

Fig. 4.22. Jerusalem-cross**.**

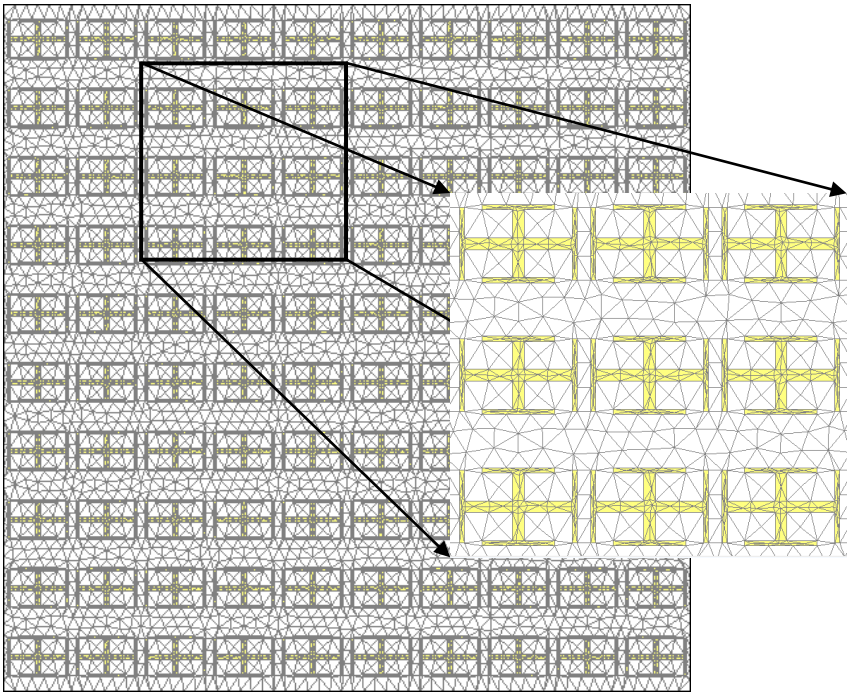

Fig. 4.23. 10 by 10 Jerusalem-cross FSS polarizer.

4.7 CHAPTER SUMMARY

In this chapter the design of a thin single-layer linear-to-circular transmission polarizer with enhanced bandwidth was presented. The starting point was a conventional Jerusalem-Cross geometry [2]. A parametric study was performed on the Jerusalem-cross unit cell. In [21] an equivalent circuit model was used to describe a Jerusalem-cross array and its performance and in this chapter the equivalent circuit model was presented. From preforming the parametric study and studying the equivalent circuit model it could be determined that by altering the dimensions of the two I-shaped structures which form the Jerusalem-cross, the two pairs of resonances due to orthogonal linear plane wave excitation of the polarizer can be controlled almost independently. By adjusting the locations of the resonances, the frequency range across which equal magnitude and a 90° phase difference is achieved can be increased. As such the circular polarization axial ratio bandwidth can also be increased. In this manner a new unit cell geometry was derived. The proposed polarizer achieves a 3 dB axial ratio bandwidth of 34%.

A numerical experiment was also presented. A 10 x 10 element Jerusalem-cross FSS polarizer was simulated using plane wave excitation and probes. The results obtained with this simulation was compared with the results obtained for the infinite array of the scaled version of the Jerusalem-cross polarizer presented in [2]. It was found that the results is a fair approximation but they do differ quite significantly and that they differ because of the different number of mesh elements used in each simulation. The more mesh elements used the better the accuracy. To simulate finite polarizers with the same accuracy used to simulate a unit cell, a large amount of memory would be required.

CHAPTER 5 MEASURED RESULTS AND COMPARISON: TRANSMISSION POLARIZER

5.1 CHAPTER OVERVIEW

This chapter presents the results achieved by the newly proposed thin single-layer linear-to-circular transmission polarizer. A comparison between simulated and measured results is shown in Section 5.2. A comparison between the simulated results of the new polarizer and the five-scaled linear-to-circular transmission polarizers studied in Chapter 3 is shown in Section 5.3.

5.2 MEASURED RESULTS

To verify the performance of the proposed polarizer a 13 × 13 element polarizer was manufactured and measured in a compact antenna range. A 13 x 13 element polarizer was required to ensure that the diffraction from the finite size polarizer has a small effect on the transmitted wave.

The transmit horn antenna in the compact antenna range feeds a parabolic reflector to provide an incident plane wave to the polarizer and receive horn antenna behind the polarizer. The polarizer is effectively in the far field of the transmit antenna. The two horn antennas are connected to a Vector network analyzer (VNA) via cables. The polarizer was placed 50 mm in front of the receiving horn antenna. Ideally both the transmit and receive antennas should be placed far away from the polarizer, but due to the fact that a finite sized polarizer is used, the receive antenna should be placed closer to the polarizer. The transmit horn antenna was

oriented at an angle of 45°, to provide a 45° linearly polarized plane wave. Two sets of measurements were performed, one with the receiving horn antenna oriented to receive linear vertical polarization and the second with the receiving horn antenna oriented to receive linear horizontal polarization. The measurement setup is shown in Fig. 5.1 and Fig. 5.2. A set of reference measurements were also performed without the polarizer.

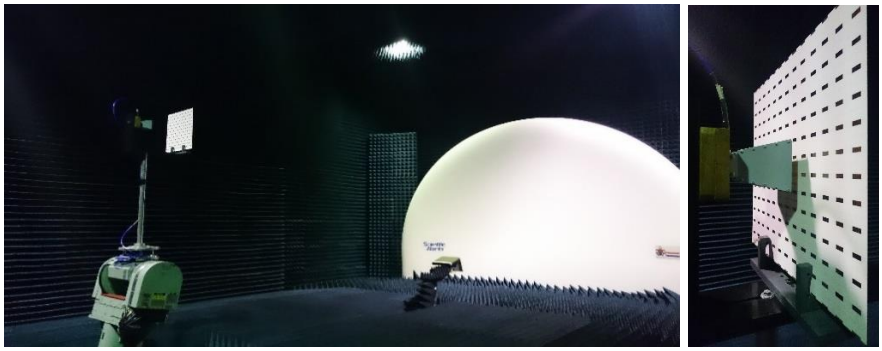

Fig. 5.1. Measurement setup.

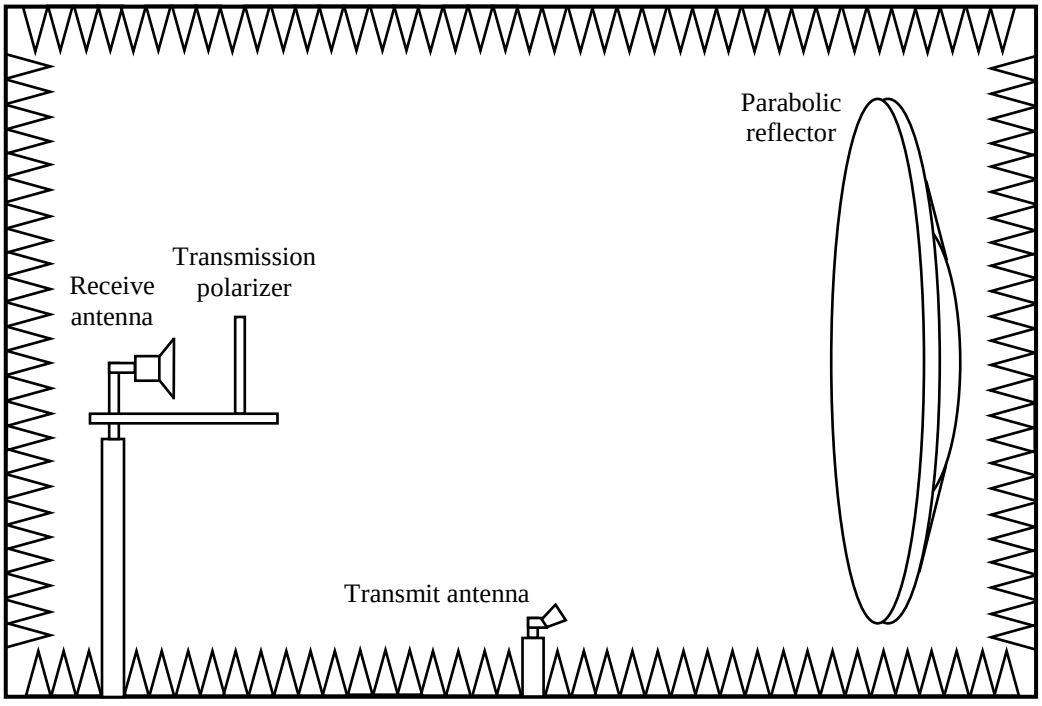

Fig. 5.2. Measurement setup in a compact antenna test range.

5.2.1 Transmission magnitude

Fig. 5.3 shows the simulated and measured transmission magnitude of the horizontal and vertical components in dB, across the 1.5 GHz to 3.5 GHz frequency range.

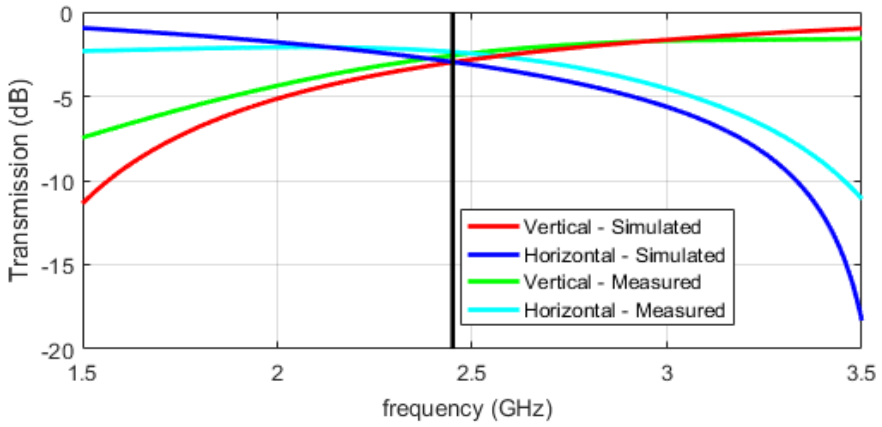

Fig. 5.3. Simulated and measured magnitude of the transmission coefficients of the vertical and horizontal components in dB. The vertical black line indicates the 2.45 GHz point where equal power transmission is required (-3 dB).

It can be seen from Fig. 5.3 that the measured point of equal magnitude for the polarizer is approximately 2.5 GHz.

5.2.2 Phase difference

Fig. 5.4 shows the simulated and measured phase difference between the horizontal and vertical components in degrees, across the 1.5 GHz to 3.5 GHz frequency range. It can be seen from Fig. 5.4 that the measured phase difference for the polarizer is within ± 8° of 90° across the 2 GHz to 3 GHz frequency range.

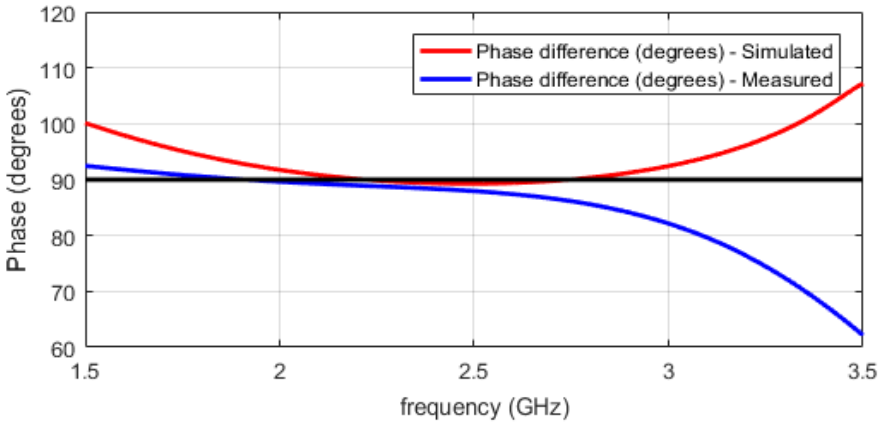

Fig. 5.4. Simulated and measured phase difference between the vertical and horizontal components in degrees. The horizontal black line marks 90° phase difference level.

5.2.3 Axial ratio

Fig. 5.5 shows the simulated and measured axial ratio in dB, across the 1.5 GHz to 3.5 GHz frequency range. The axial ratio was calculated as the ratio of the major to minor axis in both cases [2].

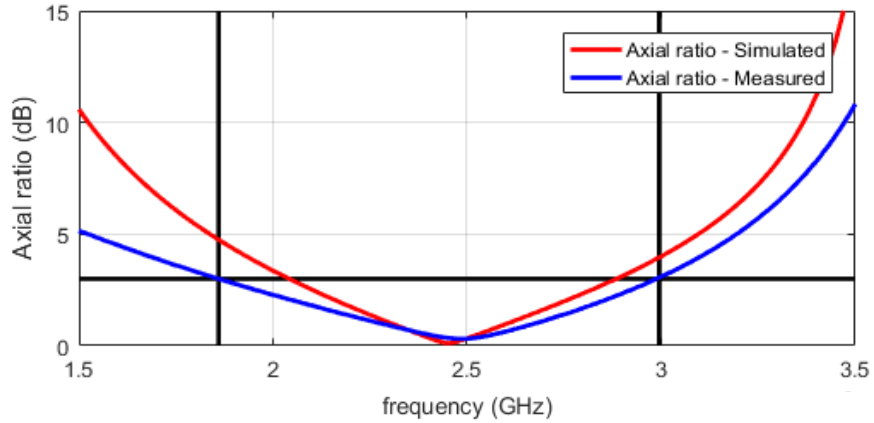

Fig. 5.5. Simulated and measured axial ratio in dB. The horizontal black line indicates the 3dB axial ratio level. The two vertical black lines represents the measured 3 dB axial ratio bandwidth.

From Fig. 5.5 it can be seen that the measured axial ratio is below 3 dB from 1.86 GHz to 2.995 GHz.

5.2.4 Discussion

It can be seen from Fig. 5.3 and Fig. 5.4 that the polarizer produces a 90° phase difference between the horizontal and vertical components of the incident wave, while maintaining equal magnitude at 2.45 GHz. Almost perfect circular polarization is obtained at 2.5 GHz. It can be seen from Fig. 5.3, Fig. 5.4 and Fig. 5.5 respectively that there is good correlation between the simulated and measured results in the 2 GHz to 3 GHz frequency range. From Fig. 5.5 it can be seen that the polarizer achieves a 3 dB axial ratio bandwidth of 46.76%, which is more than the simulated axial ratio bandwidth of 34%.

5.3 COMPARISON WITH OTHER POLARIZERS

In Table 5.1 the performance of the newly proposed polarizer is compared with the five-scaled linear-to-circular transmission polarizers studied in Chapter 3, in terms of axial ratio bandwidth, physical size and electrical size.

From Fig. 3.3 to Fig. 3.7 and Fig. 5.5, and Table 5.1 it can be seen that the proposed polarizer achieved the largest axial ratio bandwidth of 34%. This is more than double the axial ratio bandwidth achieved by the other mentioned polarizers. It can also be seen that our proposed polarizer has the smallest area of the six polarizers.

Table 5.1 Comparison of polarizers.

Polarizer	**Axial ratio bandwidth**	**Physical size (mm)**	**Electrical size (λ)**
Jerusalem-cross	10.6%	41.66 x 41.66	0.34 x 0.34
Nestled split ring slot	9.18%	67.10 x 70.64	0.55 x 0.58
Metallic ring with embedded rectangular strip	14%	55.50 x 55.50	0.45 x 0.45
Rectangular loop with diagonal microstrip	12.12%	47.06 x 47.06	0.38 x 0.38
Cross slot	10.29%	59.18 x 59.18	0.48 x 0.48
Proposed	34%	32.3 x 29.2	0.26 x 0.24

5.4 CHAPTER SUMMARY

In this chapter the measured results achieved by the newly proposed thin single-layer linear-to-circular transmission polarizer was presented. The measured axial ratio bandwidth (46.76%) was better than the simulated axial ratio bandwidth (34%). The difference between

the two sets of results are mainly due to the fact that a finite sized polarizer was used during the measurement as opposed to an infinite polariser in the simulation. A second cause for the difference is measurement error because of imperfection in the plane wave excitation or the alignment during the measurement setup. From the simulated and measured results, and the comparison with other single-layer polarizers, it can be seen that it was possible to design and manufacture a polarizer which performed better in terms of axial ratio bandwidth than other single-layer polarizers found in the literature.

CHAPTER 6 REFLECTION POLARIZER DESIGN PROCEDURE

6.1 CHAPTER OVERVIEW

This chapter focuses on the design of a thin single-layer reflective linear-to-circular polarizer with enhanced bandwidth. The starting point was a conventional ground backed Jerusalem-Cross geometry [18]. In Section 6.2 results of a parametric study performed on the ground backed Jerusalem-cross unit cell are presented. In the next section, Section 6.3, an equivalent circuit model is presented that gives some insight in the performance of the ground backed Jerusalem-cross array. In Section 6.4 a new unit cell geometry is designed. In the last section, Section 6.5, the simulation results of the new unit element are presented.

6.2 PARAMETRIC STUDY

A parametric study was performed on the ground backed Jerusalem-cross unit cell presented in [18], to determine whether an improvement in axial ratio bandwidth could be achieved. For ease of reference the unit cell will be repeated below, Fig. 6.1, with some of the dimensions indicated in the figure.

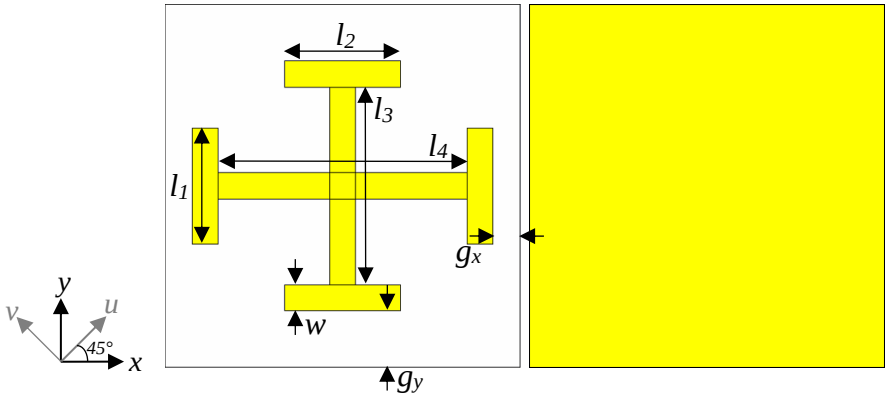

Fig. 6.1. Two perpendicular I-shaped structures on top of a ground plane unit cell. a) Front view. b) Back view [18].

6.2.1 Simulation of unit cell

Define R_{uu} and R_{uv} as the reflection coefficients of *u*- and *v*-polarized reflected waves for *u*-polarized incident waves using the coordinate system is shown Fig. 6.1.The magnitudes of the reflected electric fields $|E_u^{\mathrm{r}}|$ and $|E_v^{\mathrm{r}}|$ are given by (6.1) and (6.2) as

$$|E_u{}^r| = R_{uu}|E_u{}^i| \tag{6.1}$$

$$|E_v{}^r| = R_{uv}|E_u{}^i|. \tag{6.2}$$

The phase difference between the reflected electric fields can be calculated using (6.3).

$$\angle E_u{}^r - \angle E_v{}^r = \angle R_{uu} - \angle R_{uv} = \phi \tag{6.3}$$

In order to achieve circular polarization, the polarizer must enforce a 90° phase difference ($\angle R_{uu} - \angle R_{uv} = 90°$) and equal magnitude ($|R_{uu}| = |R_{uv}|$) on the reflected E_u^{r} and E_v^{r} components.

6.2.2 Parameter Sweep

It was decided to sweep the same parameters (l_1, l_2, g_x and g_y) which appeared to have a significant effect on the performance of the Jerusalem Cross unit cell investigated in Chapter 4 for the transmission polarizer design. For each sweep performed, the value of each dimension is given in Table 6.1. The dimensions of the reference design performed in Chapter 3 are also noted.

Table 6.1 Sweeps performed.

	l_1 (mm)	l_2 (mm)	l_3 (mm)	l_4 (mm)	w (mm)	g_x (mm)	g_y (mm)
Reference design	1.56	1.56	4.76	3.82	0.5	0.66	0.98
Sweep 1	1.56	1.56	4.76	3.82	0.5	**0.2 – 1**	0.98
Sweep 2	1.56	1.56	4.76	3.82	0.5	0.66	**0.6 – 1.4**
Sweep 3	**0.5 – 2.5**	1.56	4.76	3.82	0.5	0.66	0.98
Sweep 4	1.56	**0.5 – 2.5**	4.76	3.82	0.5	0.66	0.98

6.2.3 Parameter Sweep - Results

Fig. 6.2 (a) shows the reflection magnitude of the plus 45° (R_{uu}) and minus 45° (R_{uv}) components in dB across the 6 GHz to 13 GHz frequency range, of the reference design. Fig. 6.2 (b) shows the phase of the R_{uu} and R_{uv} components in degrees across the 6 GHz to 13 GHz frequency range.

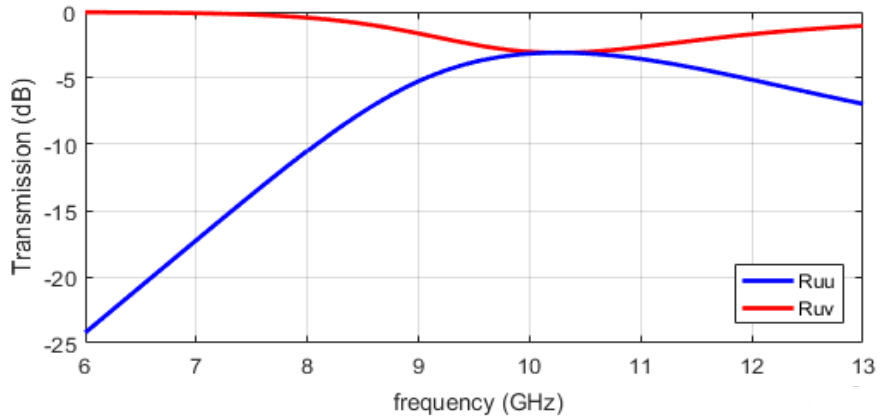

(a)

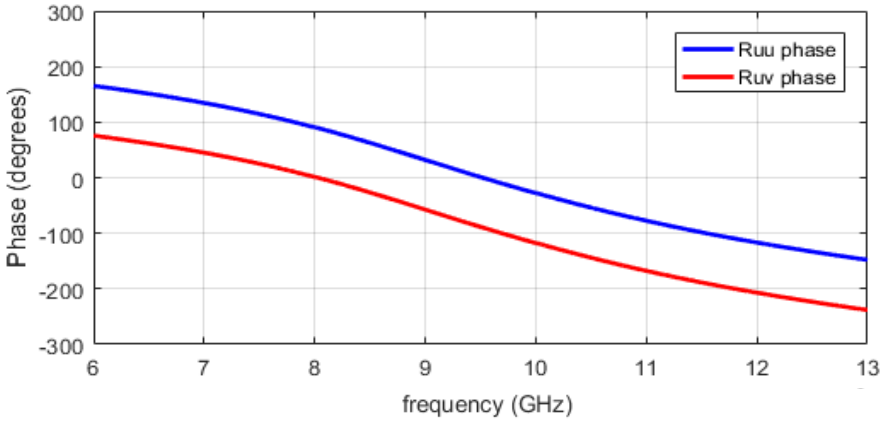

(b)

Fig. 6.2. Reflection magnitude and phase response as a function of frequency.

(a) Reflection magnitude. (b) Phase.

From Fig. 6.2 it can be concluded that the axial ratio bandwidth is manly dependent on the magnitudes of the plus 45° (R_{uu}) and minus 45° (R_{uv}) components, as the phase difference remains constant and equal to 90° across the 6 GHz to 13 GHz frequency range. The goal is to find a set of parameters which increases the range across which $|R_{uu}|$ and $|R_{uv}|$ are close to -3 dB (close to equal in magnitude).

Fig. 6.3 shows the reflection magnitude difference between the R_{uu} and R_{uv} components in dB across the 6 GHz to 13 GHz frequency range, for sweep 1 where g_x was varied from 0.2 to 1 mm.

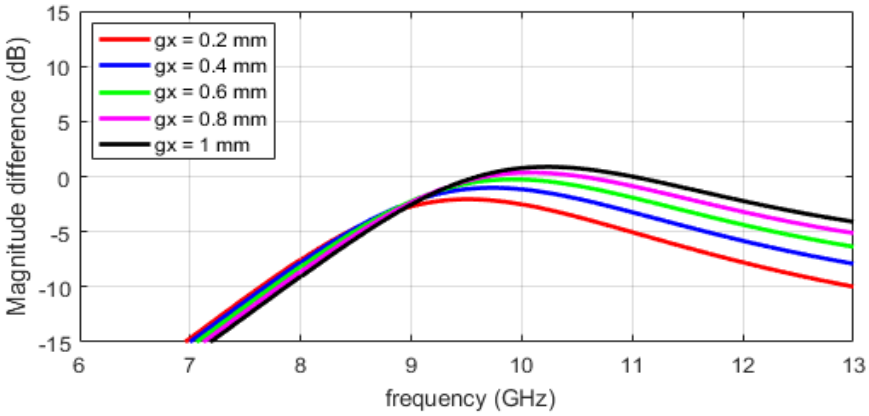

Fig. 6.3. Reflection magnitude difference as a function of frequency for different values of g_x, (sweep 1).

From Fig. 6.3 it can be seen that by increasing the value of g_x the maximum difference increases and the position moves up in frequency. It appears as if the bandwidth improves slightly for increases in values of g_x if one considers the bandwidth spanned by the maximum difference value minus some delta value (e.g. 1 dB).

Fig. 6.4 shows the reflection magnitude difference between the R_{uu} and R_{uv} components in dB across the 6 GHz to 13 GHz frequency range, for sweep 2 where g_y was varied from 0.6 to 1.4 mm.

From Fig. 6.4 it can clearly be seen that by increasing the value of g_y the magnitude difference curve flattens out and the position of the maximum difference value moves up in frequency. The bandwidth across which the magnitude difference is close to zero can be increased, if the flattened-out curve can be brought closer to zero.

Fig. 6.5 (a) shows the reflection magnitude difference between the R_{uu} and R_{uv} components in dB across the 6 GHz to 13 GHz frequency range, for sweep 3 where l_1 was varied from 0.5 to 2.5 mm.

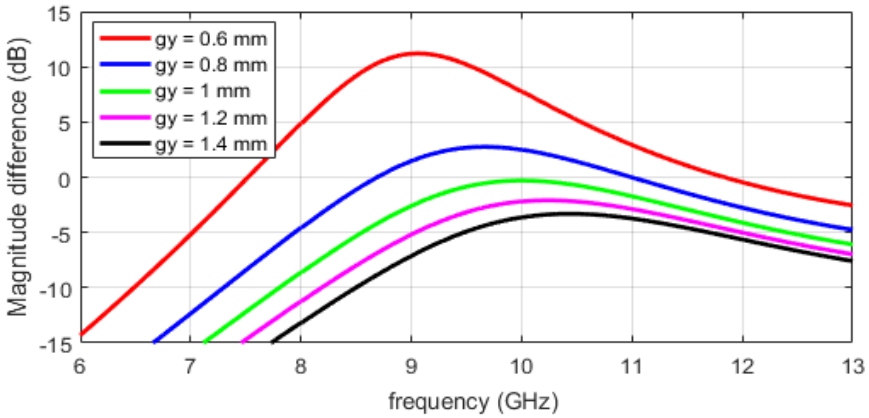

Fig. 6.4. Reflection magnitude and phase response as a function of frequency for different values of g_y, (sweep 2).

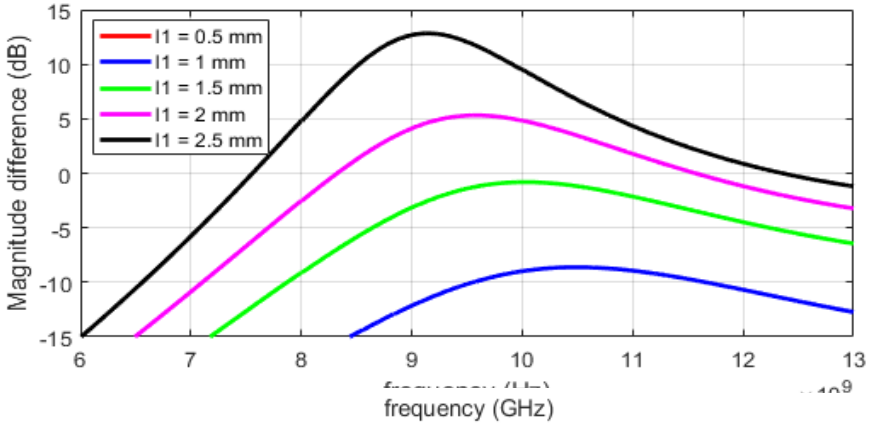

Fig. 6.5. Reflection magnitude and phase response as a function of frequency for different values of l_1, (sweep 3).

From Fig. 6.5 it can be seen that by decreasing the value of l_1 the magnitude difference curve flattens out quite significantly and the position of the maximum difference value moves up in frequency. The bandwidth across which the magnitude difference is close to zero can be increased, if the flattened curve can be brought closer to zero.

Fig. 6.6 shows the reflection magnitude difference between the R_{uu} and R_{uv} component in dB across the 6 GHz to 13 GHz frequency range, for sweep 4 where l_2 was varied from 0.5 to 2.5 mm.

From Fig. 6.6 it can be seen that by increasing the value of l_2 the position of the maximum difference value moves down in frequency (left). It appears as if the bandwidth spanned by the maximum difference value and some delta value (e.g. 1 dB) decreases as l_2 increases.

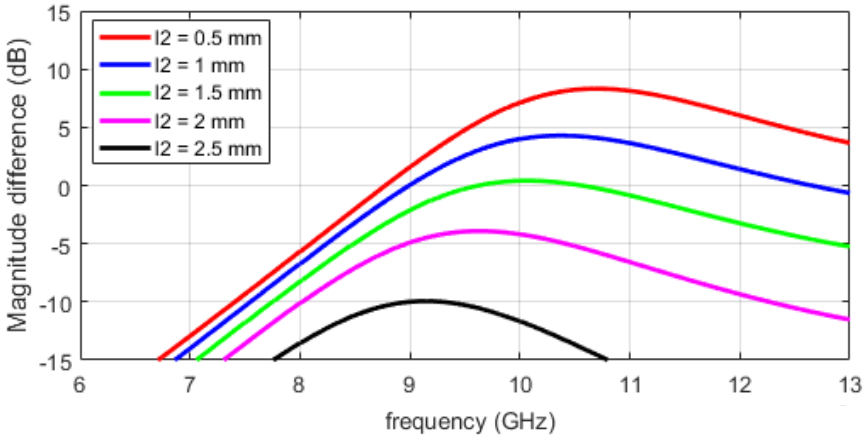

Fig. 6.6. Reflection magnitude and phase response as a function of frequency for different values of l_2, (sweep 4).

It can be seen from sweep 1 to sweep 4 and Fig. 6.2 to Fig. 6.6 that the magnitude is to some extent determined by all the parameters g_x, g_y, l_1 and l_2. By altering the values of l_1, l_2, g_x and g_y the frequency range across which a phase difference of 90°, and equal R_{uu} and R_{uv} components is achieved, can be controlled and the axial ratio bandwidth can possibly be increased if optimal values for these parameters can be determined.

6.3 EQUIVALENT CIRCUIT MODEL

An equivalent circuit, which consists of an LC circuit in parallel with an inductor, can be used to model the reflection of a vertically or horizontally polarized plane wave (normally incident) by a planar ground backed Jerusalem-cross array shown in Fig. 6.7 [22]. The equivalent circuit is shown in Fig. 6.8. When using this model, the assumption is made that $max\ (w_{cap}, w_{ind})/h < 2$, where h is the thickness of the substrate.

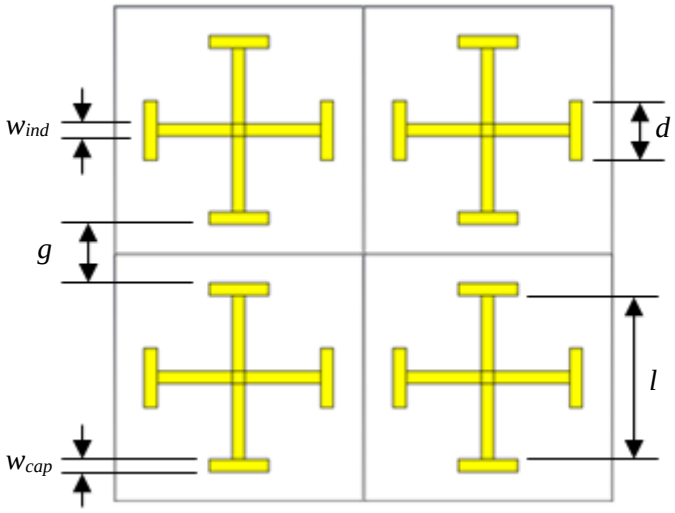

Fig. 6.7. Ground backed Jerusalem-cross array [22].

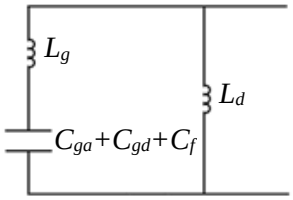

Fig. 6.8. Equivalent circuit model [22].

Using the transmission line approach, the surface impedance (as a function of angular frequency) can be expressed as a parallel connection of the grid impedance (Z_g) and the impedance of the grounded dielectric (Z_d), and is given by (6.4)

$$Z_s(\omega) = Z_g \parallel Z_d = \frac{j\omega L_d(1-\omega^2 L_g(C_{ga}+C_{gd}+C_f))}{1-\omega^2(C_{ga}+C_{gd}+C_f)(L_d+L_g)}. \tag{6.4}$$

The resonant frequency, given by (6.5), can be obtained by setting the denominator of (6.4) equal to zero. At resonance the reflection phase coefficient is zero and the surface impedance is very high.

$$f_r = \frac{1}{2\pi\sqrt{(C_{ga}+C_{gd}+C_f)(L_g+L_d)}}. \tag{6.5}$$

The calculation of L_d, L_g, C_{ga}, C_{gd} and C_f is done with microstrip equations and will be discussed below [22]. The characteristic impedance (Z_0) of a microstrip line can be calculated using (6.6)

$$Z_0 = \begin{cases} \frac{\eta}{2\pi\sqrt{\varepsilon_{re}}} \ln\left\{\frac{8h}{w} + 0.25\frac{w}{h}\right\}, & \frac{w}{h} \leq 1 \\ \frac{\eta}{\sqrt{\varepsilon_{re}}}\left\{\frac{w}{h} + 1.393 + 0.667\ln\left(\frac{w}{h} + 1.444\right)\right\}^{-1}, & \frac{w}{h} \geq 1 \end{cases}, \tag{6.6}$$

where η is the impedance of free space, h is the thickness of the dielectric slab, w is the width of the microstrip line and the effective permittivity (ε_{re}) can be calculated using (6.7)

$$\varepsilon_{re} = \frac{\varepsilon_r + 1}{2} + \frac{\varepsilon_r - 1}{2} F\left(\frac{w}{h}\right). \tag{6.7}$$

$F(w/h)$ is calculated using (6.8) [22].

$$F\left(\frac{w}{h}\right) = \begin{cases} \left(1 + \frac{12h}{w}\right)^{-\frac{1}{2}} + 0.041\left(1 - \frac{w}{h}\right)^2 & , \frac{w}{h} \leq 1 \\ \left(1 + \frac{12h}{w}\right)^{-\frac{1}{2}} & , \frac{w}{h} \geq 1 \end{cases} \tag{6.8}$$

6.3.1 Grid capacitance

In the gap between two adjacent capacitive components, specified by length d and width w_{cap}, the grid capacitance is formed. Two parallel capacitive components separated by a distance g on top of a ground plane is similar in structure to coupled line microstrip. This implies that the grid capacitance can be calculated using the equation for coupled line microstrip. C_{ga} which describes the gap capacitance in air, can be calculated using (6.9) [22]:

$$C_{ga} = 2\varepsilon_0\varepsilon_{re}\frac{K(k)}{K(k\prime)}d \tag{6.9}$$

where ε_0 is the permittivity of free space, ε_{re} can be calculated using (6.7) with w replaced by w_{cap} and $K(k)/K(k')$ can be calculated using (6.10).

$$\frac{K(k)}{K(k')} = \begin{cases} \frac{1}{\pi}\ln\left\{2\frac{1+\sqrt{k}}{1-\sqrt{k}}\right\} & ,0.707 \leq k \leq 1 \\ \frac{\pi}{\ln\left[2\frac{1+\sqrt{k'}}{1-\sqrt{k'}}\right]} & ,0 \leq k \leq 0.707 \end{cases} \tag{6.10}$$

k is given by (6.11) and *k'* is given by (6.12).

$$k = \tan^2\left(\frac{a\pi}{4b}\right) \tag{6.11}$$

$$k' = \sqrt{1-k^2} \tag{6.12}$$

a and *b* are given by (6.13) and (6.14).

$$a = \frac{w_{cap}}{2} \tag{6.13}$$

$$b = \frac{(w_{cap}+g)}{2} \tag{6.14}$$

The capacitance formed at the outer edge of the strip, also known as the fringe capacitance (C_f), can be calculated using (6.15):

$$C_f = \frac{1}{2}\left(\frac{\sqrt{\varepsilon_{re}}}{cZ_0} - \frac{\varepsilon_0\varepsilon_r w_{cap}}{h}\right) \tag{6.15}$$

where *c* is the velocity of light in free space and Z_0 is calculated using (6.6) with *w* replaced by w_{cap}.

The electric flux in the dielectric region, gives rise to capacitance C_{gd} which can be calculated using (6.16).

$$C_{gd} = \frac{\varepsilon_0\varepsilon_r}{\pi}\ln\left(\cot\left(\frac{\pi g}{4h}\right)\right) + 0.65C_f\left\{\frac{0.02h\sqrt{\varepsilon_r}}{g} + \left(1-\frac{1}{\varepsilon_r^2}\right)\right\} \tag{6.16}$$

6.3.2 Grid inductance

The grid inductance L_g, specified by length *l* and width w_{ind}, can be calculated using (6.17) and microstrip transmission line theory. The assumption is made that $l << \lambda$.

$$L_g = \frac{Z_0\sqrt{\varepsilon_{re}}}{c} l \tag{6.17}$$

Z_0 and ε_{re} can be calculated using (6.6) and (6.7) with w replaced by w_{ind}.

6.3.3 Inductance of the grounded dielectric

The inductance of the grounded dielectric, L_d, can be calculated using (6.18), if $h << 1$.

$$L_d = \mu_0 h \tag{6.18}$$

From (6.5) it can be seen that by altering the dimensions of the two I-shaped structures which form the ground backed Jerusalem-cross, the capacitance and inductance of the series resonant circuit can be controlled. The aim is to modify the capacitance and inductance to increase the frequency span across which the two components are of equal magnitude and a phase difference of 90° is achieved, and as such increase the circular polarization axial ratio bandwidth [22].

6.4 UNIT CELL DESIGN

When considering the results of the parametric study and the equivalent circuit model it is unclear how to modify the unit cells parameters to improve the axial ratio bandwidth. This is quite different to the case in Chapter 4, where it was obvious that an increase in the distance between the two resonances would result in an increase in axial ratio bandwidth. It was decided to use CST to optimize all the parameters except the width (ensure manufacturability) to increase the axial ratio bandwidth. The parameters were optimized to increase the frequency span across which the phase difference between the R_{uu} and R_{uv} components are 90° and their magnitudes are close to -3 dB (close to equal in magnitude).

The newly proposed unit cell is shown in Fig. 6.9. The substrate material is Rogers 4003C with ε_r = 3.38, tan δ = 0.0027 and thickness h = 3.861 mm. The determined dimensions are P_x = 9.82 mm, P_y = 6.14 mm, L_2 = 4.61 mm, L_3 = 3.94 mm, L_4 = 7.72 mm and W_1 = 0.5 mm.

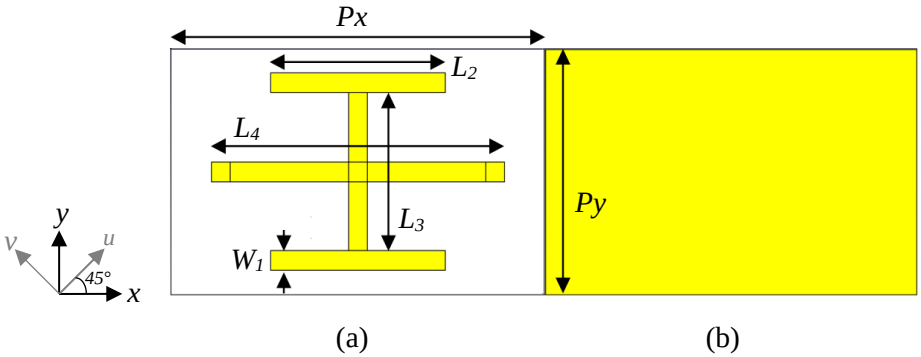

Fig. 6.9. Proposed new unit cell.

(a) Front view. (b) Back view.

6.5 CST SIMULATION

6.5.1 Simulation results of proposed unit cell

The proposed polarizer's CST simulation results are presented below.

6.5.1.1 Reflection magnitude

Fig. 6.10 shows the simulated magnitude of the reflection coefficients R_{uu} and R_{uv} in dB, across the 6 GHz to 13 GHz frequency range.

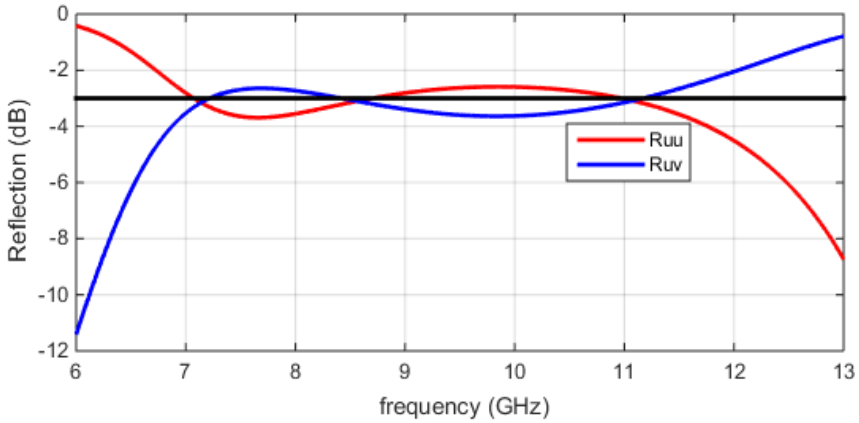

Fig. 6.10. Simulated magnitude of the reflection coefficients R_{uu} and R_{uv} in dB. The horizontal black line indicates where equal magnitude is obtained (-3 dB).

It can be seen from Fig. 6.10 that the magnitudes are within ±1 dB of -3 dB (equal in magnitude) across the 6.88 GHz to 11.76 GHz frequency range.

6.5.1.2 Phase difference

Fig. 6.11 shows the simulated phase difference between the reflection coefficients R_{uu} and R_{uv} in degrees, across the 6 GHz to 13 GHz frequency range.

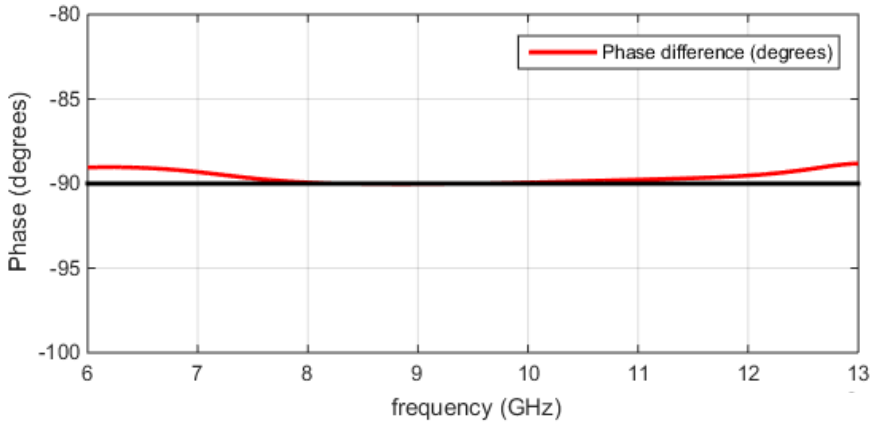

Fig. 6.11. Simulated phase difference between the reflection coefficients R_{uu} and R_{uv} in degrees. The horizontal black line marks 90° phase difference level.

It can be seen from Fig. 6.11 that the phase difference is approximately 90° across the 6 GHz to 13 GHz frequency range.

6.5.1.3 Axial ratio

The axial ratio was calculated as the ratio of the major to minor axis, using Equation 6.19 [2]. Where ϕ is the phase difference between the reflected electric fields.

$$AR = 20\log_{10}\left[\frac{\sqrt{\frac{1}{2}\left(|E_u{}^r|^2+|E_v{}^r|^2+\sqrt{|E_u{}^r|^4+|E_v{}^r|^4+2(|E_u{}^r|^2|E_v{}^r|^2\cos 2\phi)}\right)}}{\sqrt{\frac{1}{2}\left(|E_u{}^r|^2+|E_v{}^r|^2-\sqrt{|E_u{}^r|^4+|E_v{}^r|^4+2(|E_u{}^r|^2|E_v{}^r|^2\cos 2\phi)}\right)}}\right] \quad (6.19)$$

Fig. 6.12 shows the axial ratio in dB, across the 6 GHz to 13 GHz frequency range.

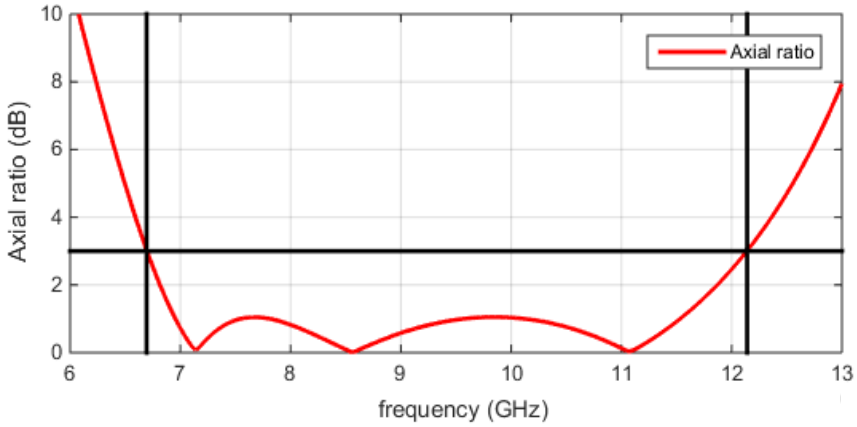

Fig. 6.12. Simulated axial ratio in dB. The horizontal black line indicates the 3dB axial ratio level. The two vertical black lines represents the 3 dB axial ratio bandwidth.

It can be seen from Fig. 6.12 that the axial ratio is below 3 dB across the 6.69 GHz to 12.14 GHz frequency range.

6.5.1.4 Discussion

It can be seen from Fig. 6.10, Fig. 6.11 and Fig. 6.12 that the proposed polarizer enforces a 90° phase difference between the components of the reflected wave, while maintaining equal magnitude, almost perfect circular polarization is obtained at 7.14 GHz, 8.56 GHz and 11.08 GHz. From Fig. 6.12 it can be seen that the proposed polarizer achieves a 3 dB axial ratio bandwidth of 57%.

6.6 CHAPTER SUMMARY

In this chapter the design of a thin single-layer reflective linear-to-circular polarizer with enhanced bandwidth is presented. The starting point was a conventional ground backed Jerusalem-Cross geometry [18]. A parametric study was performed on the ground backed Jerusalem-cross unit cell. In [22] an equivalent circuit model was used to describe a ground backed Jerusalem-cross array and its performance, this equivalent circuit model was presented above. From the parametric study and studying the equivalent circuit model it could be determined that by altering the dimensions of the two I-shaped structures which form the Jerusalem-cross, the magnitude and phase due to orthogonal linear plane wave

excitation of the polarizer can be controlled. By controlling the equal magnitude point and the phase difference a more broadband axial ratio bandwidth for the reflected circular polarized wave can be achieved. In this manner a new unit cell was designed. The polarizer achieves a 3 dB axial ratio bandwidth of 57%.

CHAPTER 7 MEASURED RESULTS AND COMPARISON: REFLECTIVE POLARIZER

7.1 CHAPTER OVERVIEW

This chapter presents the results achieved by the proposed thin single-layer reflective linear-to-circular polarizer. A comparison between simulated and measured results is shown in Section 7.2. A comparison between simulated results and the polarizer presented in [18] is shown in Section 7.3.

7.2 MEASURED RESULTS

To verify the performance of the proposed polarizer a 42 x 40 element reflective polarizer was fabricated and measured in a compact antenna range. A 42 x 40 element polarizer was required to ensure that almost all of the incident waves are reflected back to the parabolic reflector.

For the measurement two horn antennas were used. The transmit horn antenna in the compact antenna range feeds a parabolic reflector to provide an incident plane wave to the reflective polarizer, while the other antenna is used to receive the wave reflected by the polarizer and the parabolic reflector. The polarizer works in the far field. The two horn antennas are connected to a VNA via cables. The transmit horn antenna was oriented at an angle of 45°, to provide a *u*-polarized plane wave which will be reflected by the polarizer. Two sets of measurements were performed, one with the receiving horn antenna oriented to receive *u*-polarization and the second with the receiving horn antenna oriented to receive *v*-

polarization, to obtain the R_{uu} and R_{uv} reflection coefficients. The measurement setup is shown in Fig. 7.1. A set of reference measurements were also performed with the ground plane of the polarizer. Time gating was used to eliminate cross-talk between the transmit and receive antennas during the measurements.

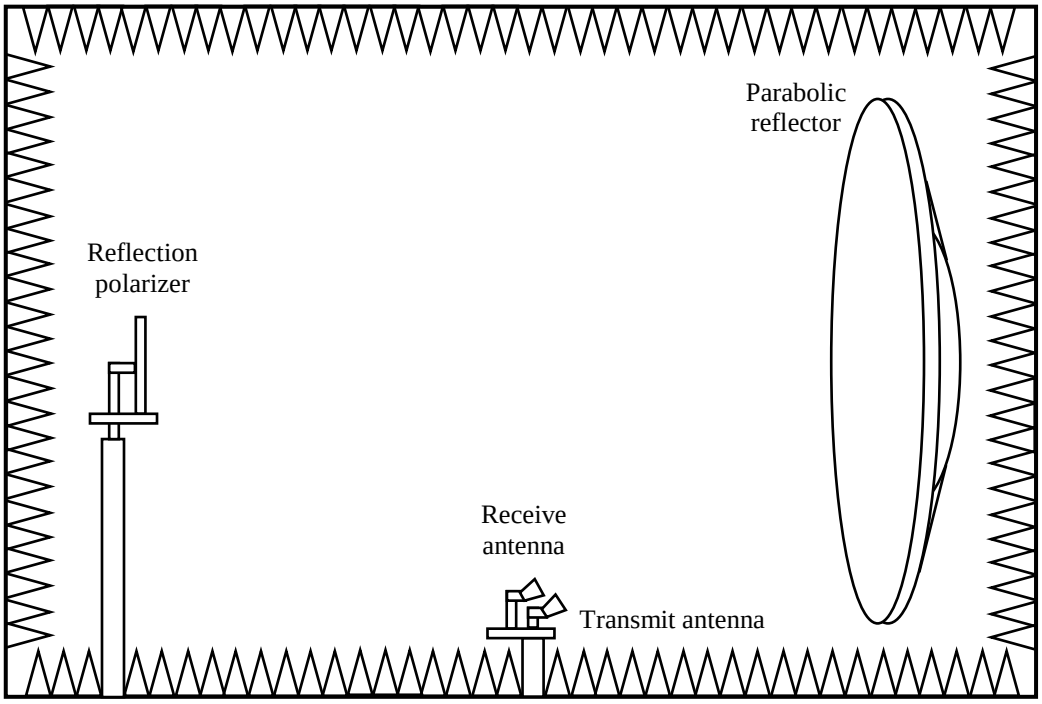

Fig. 7.1. Measurement setup in a compact antenna test range.

7.2.1 Reflection magnitude

Fig. 7.2 shows the simulated and measured magnitude of the reflection coefficients R_{uu} and R_{uv}, across the 6 GHz to 13 GHz frequency range. It can be seen from Fig. 7.2 and the measured data that the magnitudes are within ±1 dB of -3 dB (equal in magnitude) across the 6.88 GHz to 11.76 GHz frequency range.

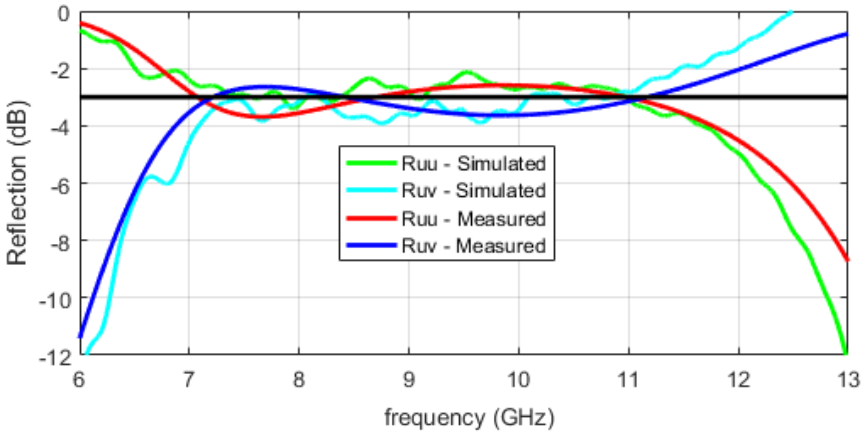

Fig. 7.2. Simulated and measured magnitude of the reflection coefficients R_{uu} and R_{uv} in dB. The horizontal black line indicates where equal magnitude is located (-3 dB).

7.2.2 Phase difference

Fig. 7.3 shows the simulated and measured phase difference between the reflection coefficients R_{uu} and R_{uv}, across the 6 GHz to 13 GHz frequency range. It can be seen from Fig. 7.3 and the measured data that the phase difference is within ±3° of 90° across the 6 GHz to 13 GHz frequency range for the polarizer.

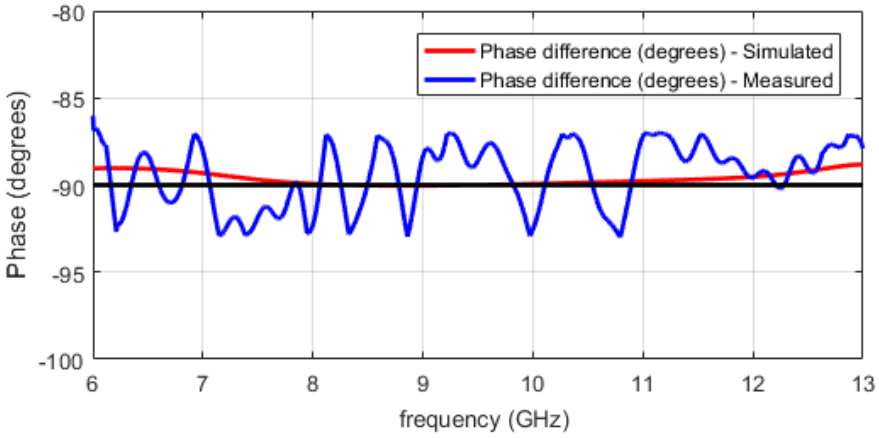

Fig. 7.3. Simulated and measured phase difference between the reflection coefficients R_{uu} and R_{uv} in degrees. The horizontal black line marks 90° phase difference level.

7.2.3 Axial ratio

Fig. 7.4 shows the simulated and measured axial ratio, across the 6 GHz to 13 GHz frequency range. In both cases the axial ratio was calculated as the ratio of the major to minor axis [2].

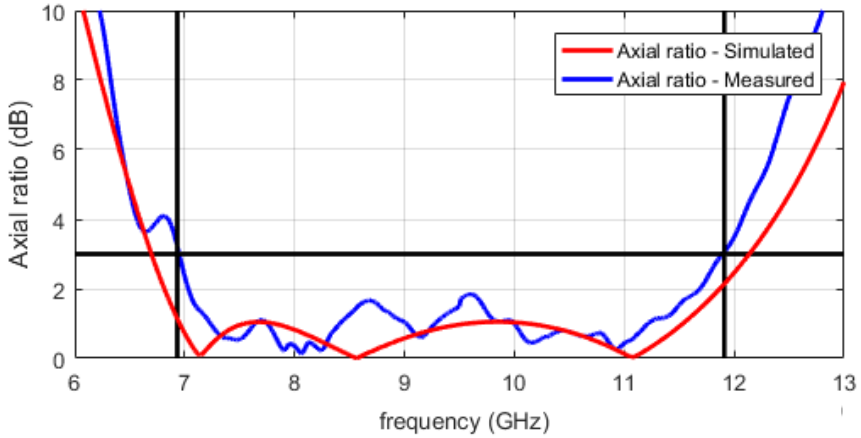

Fig. 7.4. Simulated and measured axial ratio in dB. The horizontal black line indicates the 3dB axial ratio level. The two vertical black lines represents the 3 dB axial ratio bandwidth.

From Fig. 7.4 it can be seen that the measured axial ratio is below 3 dB from 6.933 GHz to 11.91 GHz.

7.2.4 Discussion

It can be seen from Fig. 7.2 and Fig. 7.3 that the proposed polarizer produces a 90° phase difference between the components of the incident wave, while maintaining equal magnitude, and almost perfect circular polarization is obtained at 7.14 GHz and 11.08 GHz. It can be seen from Fig. 7.2, Fig. 7.3 and Fig. 7.4 respectively that there is good correlation between the simulated and measured results in the 7 GHz to 12 GHz frequency range. It can be seen from Fig. 7.4 that the proposed polarizer achieves a 3 dB axial ratio bandwidth of 52.8%, which is slightly less than the simulated axial ratio bandwidth of 57%.

7.3 COMPARISON WITH OTHER POLARIZERS

In Table 7.1 the proposed polarizer is compared to the ground backed Jerusalem-cross polarizer presented in [18], in terms of axial ratio bandwidth, substrate height, physical size and electrical size.

Table 7.1 Comparison of polarizers.

Polarizer	**Axial ratio bandwidth**	**Substrate height in mm**	**Physical size in mm**	**Electrical size in wavelengths**
Ground backed Jerusalem-cross	26.73%	3	6.93 x 6.78	0.238 x 0.233
Proposed	57%	3.861	9.82 x 6.14	0.308 x 0.193

From Fig. 3.8, Fig. 7.4 and Table 7.1 it can be seen that the proposed polarizer achieved the largest axial ratio bandwidth of 57% which is more than double the axial ratio bandwidth achieved by the ground backed Jerusalem-cross polarizer. It can also be seen that the proposed polarizer has a slightly larger thickness. This increase facilitated the larger axial ratio bandwidth.

7.4 CHAPTER SUMMARY

In this chapter the measured results achieved by the newly proposed thin single-layer reflective linear-to-circular polarizer was presented. From the simulated results, measured results and the comparison with another single-layer polarizer, it can be seen that it was possible to design and manufacture a polarizer which performed better in terms of axial ratio bandwidth than other reflective single-layer polarizers found in the literature.

CHAPTER 8 CONCLUSION

8.1 SUMMARY OF WORK

The objective of this dissertation was to design two thin single-layer linear-to-circular polarizers, one for transmission and the other for reflection, with enhanced bandwidth. The two polarizers had to perform better, in terms of axial ratio bandwidth, then other single-layer linear-to-circular polarizers found in the literature.

The literature study conducted in Chapter 2 on transmission linear-to-circular polarizers revealed that there was still a need for a thin transmission single-layer linear-to-circular polarizer with enhanced bandwidth. Chapter 2 also revealed that reflective linear-to-linear polarizers have been studied extensively and that it would not be an easy task to improve the bandwidth of these polarizes. It was found that reflective linear-to-circular polarizers have not been studied as thoroughly and that there was a need for a thin reflective single-layer linear-to-circular polarizer with enhanced bandwidth.

In Chapter 3 the performance of the linear-to-circular polarizers mentioned in Section 2.4 and Section 2.5, was studied and compared. The performance of these polarizers was studied to determine what kind of bandwidth polarizers in the literature achieve.

In Chapter 4 a thin single-layer linear-to-circular transmission polarizer with enhanced bandwidth was designed. The starting point was the conventional Jerusalem-cross geometry. A parametric study was performed on the Jerusalem-cross unit cell. An equivalent circuit used to describe a Jerusalem-cross array in the literature, was presented. From the resonance frequency equation and the parametric study, it could be seen that by altering the dimensions

of the two I-shaped structures which form the Jerusalem-cross, the position of the transmission zeros, could be controlled. The locations of the resonances were adjusted to increase the frequency range across which equal magnitude, and a 90°, is achieved, and as such increase the circular polarization axial ratio bandwidth. In this manner a new unit cell was derived.

In Chapter 5 the measured results achieved by the proposed thin single-layer linear-to-circular transmission polarizer was presented. A comparison between the simulated and measured results was made which indicated that there is good correlation between the simulated and measured results. A comparison between the proposed polarizers simulated results and polarizers presented in literature was also shown.

In Chapter 6 a thin reflective single-layer linear-to-circular polarizer with enhanced bandwidth was designed. The starting point was a ground backed Jerusalem-cross. A parametric study was performed on the ground backed Jerusalem-cross. An equivalent circuit used to describe a ground backed Jerusalem-cross array in the literature, was presented. From studying the equivalent circuit and performing the parametric study, it could be seen that by altering the dimensions of the two I-shaped structures which form the Jerusalem-cross, the magnitude and phase response, could be controlled. The frequency range across which a phase difference of 90°, and equal magnitude components is achieved was increased by altering the dimensions of the two I-shaped structures, and as such the circular polarization axial ratio bandwidth was also increased. In this manner a new unit cell was designed.

In Chapter 7 the measured results achieved by the proposed thin reflective single-layer linear-to-circular polarizer was presented. There is good correlation between the simulated and measured results. A comparison between the simulated results and a polarizer in the literature was also shown.

In conclusion two thin single-layer linear-to-circular polarizers, one for transmission and the other for reflection, with enhanced bandwidth was designed. The two polarizers perform better than most existing single-layer linear-to-circular polarizers, in terms of axial ratio bandwidth. The hypothesis that altering the geometry of the unit cell, to increase the bandwidth of the unit cell, will also increase the bandwidth of the linear-to-circular polarizer was proven true.

After completion of these designs, it was found that an improved reflective polarizer had recently been proposed. The polarizer was also derived from a ground backed Jerusalem-cross and achieves similar performance to the reflective polarizer presented in this thesis. The polarizer consists of a micro-split Jerusalem-cross unit cell and achieves a 3 dB axial ratio bandwidth of 50% [23].

8.2 CONTRIBUTION

A short summary of the contributions made by this study is given below:

- A thin linear-to-circular transmission polarizer with enhanced bandwidth was designed.
- A comparison was made between existing thin single-layer transmission polarizers and the proposed polarizer.
- A thin reflective linear-to-circular polarizer with enhanced bandwidth was designed.
- A comparison was made between an existing thin reflective linear-to-circular polarizer and the proposed polarizer.

8.3 FUTURE WORK

While conducting this study the following possible future research with regard to thin single-layer polarizers were identified:

Investigate performance of the proposed transmission and reflective polarizers under oblique incidence: The performance of the linear-to-circular transmission and reflective polarizers could be investigated under oblique incidence to determine the usable range of the polarizer.

Incorporate the proposed transmission and reflective polarizers with a planar antenna: A study could be done to determine if the polarization and the performance of a planar antenna can be improved by incorporating the proposed linear-to-circular transmission and reflective polarizers.

Reduce the size of the unit cell: A study could be done to determine if it would be possible and have any benefit to reduce the size of the proposed polarizer's unit cells by incorporating meander line, or using v-shaped wires.

REFERENCES

[1] X. Ma, C. Huang, M. Pu, C. Hu, Q. Feng and X. Luo, "Single-layer circular polarizer using metamaterial and its application in antenna," *Microwave and Optical Technology letters,* vol. 54, no. 7, pp. 1770-1774, 2012.

[2] I. Sohail, Y. Ranga, K. Esselle and S. Hay, "A linear to circular polarization converter based on jerusalem-cross frequency selective surface," in *European conference on antennas and propagation (EuCAP),* pp. 2141-2143, 2013.

[3] C. L. Holloway, E. F. Kuester, J. A. Gordon, J. O'Hara, J. Booth and D. R. Smith, "An Overview of the Theory and Application of Metasurfaces: The Two-Dimensional Equivalents of Metamaterials," *IEEE Antennas and Propagation,* vol. 54, no. 2, pp. 10-11, 2012.

[4] Y. Ye and S. He, "90° polarization rotator using a bilayered chiral metamaterial with giant optical activity," *Applied Physics Letters,* vol. 96, no. 203501, pp. 1-3, 2010.

[5] Z. Wei, Y. Cao, Y. Fan, X. Yu and H. Li, "Broadband polarization transformation via enhanced asymmetric transmission through arrays of twisted complementary split-ring resonators," *Applied Physics Letters,* vol. 99, no. 221907, pp. 1-3, 2011.

[6] J. Shi, H. Ma, C. Guan, Z. Wang and T. Cui, "Broadband chirality and asymmetric transmission in ultrathin 90°-twisted Babinet-inverted metasurfaces," *Physical Review B,* vol. 89, no. 165128, pp. 1-7, 2014.

[7] H. Zhu, S. Cheung, K. Chung and T. Yuk, "Linear-to-circular polarization conversion using metasurface," *IEEE Transactions on Antennas and Propagation,* vol. 61, no. 9, pp. 4615-4623, 2013.

[8] M. Euler, V. Fusco, R. Cahill and R. Dickie, "325 GHz single layer sub-millimetre wave FSS based split slot ring linear to circular polarization convertor," *IEEE Transactions on antennas and propagation,* vol. 58, no. 7, pp. 2457-2459, July 2010.

[9] K. Kandasamy, B. Majumder, J. Mukherjee and K. Ray, "Low RCS and polarization Reconfigurable Antenna using Cross Slot Based MZetasurface," *IEEE Antennas and Wireless Propagation letters,* vol. 14, pp. 1638-1641, March 2015.

[10] Y. Li, J. Zhang, S. Qu, J. Wang, L. Zheng, Y. Pang, Z. Xu and A. Zhang, "Achieving wide-band linear-to-circular polarization conversion using ultra-thin bi-layered metasurfaces," *Journal of Applied Physics,* vol. 117, no. 044501, pp. 1-7, 2015.

[11] L. Martinez-Lopez, J. Rodriguez-Cuevas, I. Martinez-Lopez and A. Martynyuk, "A Multilayer Circular Polarizer Based on Bisected Split-Ring Frequency Selective Surfaces," *IEEE Antennas and Wireless Propagation Letters,* vol. 13, pp. 153-156, January 2014.

[12] H. Chen, J. Wang, H. Ma, S. Qu, J. Zhang, Z. Xu and A. Zhang, "Broadband perfect polarization conversion metasurfaces," *Chinese Physics B,* vol. 24, no. 1 (014201), pp. 1-5, 2015.

[13] H. Chen, J. Wang, H. Ma, S. Qu, Z. Xu, A. Zhang, M. Yan and Y. Li, "Ultra-wideband polarization conversion metasurfaces based on multiple plasmon resonances," *Journal of Applied Physics,* vol. 115, no. 154504, pp. 1-5, 2014.

[14] C. Chen, Z. Li, L. Liu, J. Xu, P. Ning, B. Xu, X. Chen and C. Gu, "A Circularly-Polarized Metasurfaced Dipole Antenna with Wide Axial-Ratio Beamwidth and RCS Reduction Functions," *Progress in Electromagnetic Research,* vol. 154, pp. 79-85, 2015.

[15] J. Yin, X. Wan, Q. Zhang and T. Cui, "Ultra Wideband Polarization-Selective Conversions of Electromagnetic Waves by Metasurface under Large-Range Incident Angles," *Scientific Reports,* vol. 5, no. 12476, pp. 1-10, 2015.

[16] H. Chen, H. Ma, S. Qu, J. Wang, Y. Li, H. Yuan and Z. Xu, "Ultra-Wideband Polarization Conversion Metasurfaces," in *3rd Asia-Pacific Conference on Atennas and Propagation,* pp. 1009-1011, 2014.

[17] Y. Liu, K. Li, Y. Jia, Y. Hao, S. Gong and Y. Guo, "Wideband RCS Reduction of a Slot Array Antenna Using Polarization Conversion Metasurfaces," *IEEE Transactions on Antennas and Propagation,* vol. 64, no. 1, pp. 326-331, 2016.

[18] H. Ma, G. Wang, G. Kong and T. Cui, "Broadband circular and linear polarization conversions realized by thin birefringent reflective metasurfaces," *Optical Materials Express,* vol. 4, no. 8, pp. 1717-1724, 2014.

[19] B. Lin, J. Wu and X. Da, "Linear-to-circular polarization converter based on a second-order band-pass frequency selective surface," *Applied Physics A,* vol. 123, no. 1, p. 43, 2017.

[20] CST, "CST- Computer Simulation Technology," Dassault Systemes, 2002-2017. [Online]. Available: https://www.cst.com/. [Accessed 30 november 2016].

[21] R. J. Langley and A. J. Drinkwater, "Improved empirical model for the Jerusalem cross," *Microwaves, Optics and Antennas, IEE Proceedings H,* vol. 129, no. 1, pp. 1-6, 1982.

[22] M. Hosseinipanah and Q. Wu, "Equivalent Circuit Model for Designing of Jerusalem Cross-Based Artificial Magnetic Conductors," *Radioengineering,* vol. 18, no. 4, pp. 544-550, 2009.

[23] X. Gao, Y. Xing-Yang, C. Wei-Ping, J. Yan-Nan and Y. Xin-Hua, "Ultra-wideband circular-polarization converter with micro-split Jerusalem-cross metasurfaces," *Chinese Physics B,* vol. 25, no. 12 (128102), pp. 1-7, 2016.